Pseudo-Dirac neutrinos in the new standard model

André de Gouvêa and Wei-Chih Huang

Department of Physics and Astronomy, Northwestern University, 2145 Sheridan Road, Evanston, Illinois 60208, USA

James Jenkins

Elementary Particles and Field Theory Group, MS B285, Los Alamos National Laboratory, Los Alamos, New Mexico 87545, USA
and Department of Physics and Astronomy, Northwestern University, 2145 Sheridan Road, Evanston, Illinois 60208, USA

The addition of gauge-singlet fermions to the standard model Lagrangian renders the neutrinos massive and allows one to explain all that is experimentally known about neutrino masses and lepton mixing by varying the values of the Majorana mass parameters M for the gauge singlets and the neutrino Yukawa couplings λ. Here we explore the region of parameter space where M values are much smaller than the neutrino Dirac masses λv. In this region, neutrinos are pseudo-Dirac fermions. We find that current solar data constrain M values to be less than at least 10^{-9} eV, and discuss the sensitivity of future experiments to tiny gauge-singlet fermion masses. We also discuss a useful basis for analyzing pseudo-Dirac neutrino mixing effects. In particular, we identify a simple relationship between elements of M and the induced enlarged mixing matrix and new mass-squared differences. These allow one to directly relate bounds on the new mass-squared differences to bounds on the singlet fermion Majorana masses.

I. INTRODUCTION

Nonzero neutrino masses reveal that the minimum standard model needs to be modified. Current data (mostly from solar, atmospheric, reactor, and accelerator neutrino oscillation experiments), however, provide only minimal insight as to *how* the standard model ought to be extended. Several completely different new physics scenarios can be constructed and all safely agree with observations; i.e., all lead to small neutrino masses and nontrivial mixing among the three so-called active neutrino weak eigenstates, ν_e, ν_μ, and ν_τ. Additions to the standard model that fit the data include right-handed neutrinos, $SU(2)_L$ triplet fermions or scalars, leptoquarks, etc. Recent summaries of the current experimental and theoretical situation can be found, for example, in [1–7].

One version for the new standard model, νSM, consists of the minimum standard model augmented by a few (at least two) $SU(2)_L \times U(1)_Y$ gauge-singlet Weyl fermions N, normally referred to as right-handed neutrinos. At the renormalizable level, the most general νSM Lagrangian consistent with $SU(3)_c \times SU(2)_L \times U(1)_Y$ gauge invariance is

$$\mathcal{L}_{\nu\text{SM}} = \mathcal{L}_{\text{old}} - \lambda_{\alpha i} L^\alpha H N^i - \sum_{i,j=1}^{n} \frac{M_{ij}}{2} N^i N^j + \text{H.c.},$$

(1.1)

where $\mathcal{L}_{\text{old}}$ is the minimal standard model Lagrangian, L are the $SU(2)_L$ lepton doublet fields $L = (\nu \ell)^T$, and H is the standard model Higgs doublet field. $\lambda_{\alpha i}$ are neutrino Yukawa couplings and M_{ij} are Majorana masses for the N fields. Note that M is a symmetric matrix: $M_{ij} = M_{ji}$. $\alpha = e, \mu, \tau$, $i = 1, \dots n$, and $n \geq 2$ is the number of right-

handed neutrino fields. After electroweak symmetry breaking, Eq. (1.1) describes $3 + n$ Majorana neutral fermions, referred to as neutrinos. In general, all neutrino mass eigenstates $\nu_1, \nu_2, \dots, \nu_{3+n}$ (with mass $m_1, m_2, \dots, m_{3+n}$) are linear combinations of the active neutrinos plus the n right-handed neutrinos. Since these singlet fermions do not couple to any of the standard model gauge bosons, they will also be referred to as sterile neutrinos.

The phenomenology associated to Eq. (1.1) depends dramatically on the values of the νSM parameters λ and M (see, for example, [8]). Even after the current data are taken into account, the spectrum of possibilities remains vast. When the matrix M vanishes exactly, the six[1] neutral states fuse into three Dirac fermions with masses proportional to the (square roots of the) eigenvalues of $\lambda^\dagger \lambda$. In this case, the classical global symmetry of $\mathcal{L}_{\nu\text{SM}}$ is enhanced and includes the lepton-number symmetry $U(1)_L$ [and its nonanomalous cousin $U(1)_{B-L}$]. This indicates that M can be interpreted as a symmetry breaking parameter (when $\lambda \neq 0$) so that (i) quantum corrections to M are proportional to M itself and hence (ii) *any* value of M is technically natural.

When $M \neq 0$, one can identify three qualitatively distinct regions of the λ, M parameter space. In the region where $M \gg \lambda v$,[2] where v is the vacuum expectation value of the neutral component of H, the six neutrino masses "split" into three lighter, mostly active states with masses

---

[1]For the remainder of this section, we restrict our discussion to $n = 3$ right-handed neutrinos.
[2]Beware of the abuse of notation and keep in mind that λ and M are matrices. For a more detailed discussion of this so-called seesaw limit, see, for example, [9].

generically of order $\lambda^2 v^2/M$ and three heavier, mostly sterile states with masses M. This phenomenon is referred to as the seesaw mechanism [10], and it was argued in [8] that all values of $M \gtrsim 1$ eV are phenomenologically allowed. For small enough M (in general M much smaller than the weak scale), the νSM can be tested experimentally since the mostly sterile, heavier states are accessible at different facilities (see, for example, [9,11,12]). It has also been pointed out that the mostly heavy states may qualify as viable warm dark matter [13]. Finally, for extraordinary choices of λ (for recent discussions see [14,15]), mostly sterile neutrinos with weak-scale masses can be detected at high-energy collider experiments.

The other two distinct regions of the λ, M parameter space are characterized by $M \sim \lambda v$ and $M \ll \lambda v$. In the former, all six neutrino masses are of the same order, and all six neutrino mass eigenstates are characterized by "homogeneous" mixtures of active and sterile flavors. Such a scenario is both hard to study quantitatively and severely constrained by current solar and atmospheric neutrino data. In this paper, we explore the latter possibility: right-handed neutrino Majorana masses M much *smaller* than the so-called Dirac neutrino masses λv. Under these circumstances, neutrinos are pseudo-Dirac fermions [16–18].

Pseudo-Dirac neutrinos are Majorana neutrinos made up of roughly fifty-fifty mixtures of active and sterile neutrinos, and come in quasidegenerate pairs. These will be properly defined in Sec. II. In the limit $M \rightarrow 0$, neutrinos are Dirac fermions and hence can accommodate all current experimental data (as discussed above), so our main goal is to estimate an upper bound for M. Given our current understanding of neutrinos, the most stringent constraints on very small M values are provided by solar data. The data, the estimation procedure, and our results are presented in Sec. III. Other constraints and predictions, as well as expectations for the future, are discussed in Sec. IV. A summary of what is currently known about pseudo-Dirac νSM neutrinos and the νSM Lagrangian [Eq. (1.1)] in general is presented in Sec. V.

II. "ANTISEESAW": MASSES AND MIXING

In the case of $n = 3$ right-handed neutrinos, after electroweak symmetry breaking, the 6×6 Majorana neutrino mass matrix is

$$M_\nu = \begin{pmatrix} 0_3 & m \\ m^T & \epsilon_m \end{pmatrix}, \qquad (2.1)$$

where 0_3 stands for the 3×3 zero matrix,

$$\epsilon_m = \epsilon_m^T = V_R^T \epsilon_m^D V_R \qquad (2.2)$$

is the symmetric 3×3 Majorana right-handed neutrino mass matrix, and we choose the weak basis where the 3×3 Dirac neutrino mass matrix is written as

$$m = U^* m^D. \qquad (2.3)$$

This can be achieved by redefining the right-handed neutrino fields N. Above, the superscript D indicates a diagonal matrix while V_R and U are unitary matrices.

Since we are interested in the limit $m^D \gg \epsilon_m^D$—Dirac masses much larger than Majorana right-handed neutrino masses—we can write

$$\begin{aligned} M_\nu &\simeq \begin{pmatrix} 1_3 & -\delta^* \\ \delta^T & 1_3 \end{pmatrix} \frac{1}{\sqrt{2}} \begin{pmatrix} U^* & -U^* \\ 1_3 & 1_3 \end{pmatrix} \\ &\times \begin{pmatrix} m^D(1_3 + \epsilon^D) & 0_3 \\ 0_3 & -m^D(1_3 - \epsilon^D) \end{pmatrix} \frac{1}{\sqrt{2}} \\ &\times \begin{pmatrix} U^\dagger & 1_3 \\ -U^\dagger & 1_3 \end{pmatrix} \begin{pmatrix} 1_3 & \delta \\ -\delta^\dagger & 1_3 \end{pmatrix}, \end{aligned} \qquad (2.4)$$

where 1_3 is the 3×3 unit matrix, and the elements of δ are small (this will be shown *a posteriori*) so that

$$\begin{pmatrix} 1_3 & \delta \\ -\delta^\dagger & 1_3 \end{pmatrix} \begin{pmatrix} 1_3 & -\delta \\ \delta^\dagger & 1_3 \end{pmatrix} = \begin{pmatrix} 1_3 & 0_3 \\ 0_3 & 1_3 \end{pmatrix} + \mathcal{O}(\delta\delta^\dagger, \delta^\dagger\delta). \qquad (2.5)$$

ϵ^D is a diagonal dimensionless matrix of small numbers. Equation (2.4) is satisfied, at leading order, if

$$\delta = U\left(\frac{\epsilon^D}{2} + \varepsilon\right), \qquad (2.6)$$

where ε is a dimensionless matrix of small numbers whose diagonal elements vanish. Both ϵ^D and ε are functions of ϵ_m and m^D:

$$\epsilon_m = 2\epsilon^D m^D + \varepsilon^T m^D + m^D \varepsilon, \qquad (2.7)$$

and

$$m^D \varepsilon^T = -\varepsilon m^D. \qquad (2.8)$$

Note that m^D and ε do not commute and that ϵ_m is indeed a symmetric matrix with units of mass. Throughout we will ignore the possibility, ruled out by data, that different diagonal entries of m^D are identical. According to Eq. (2.7), in the weak basis of choice and at leading order, the diagonal elements of ϵ_m, proportional to ϵ^D, determine the mass-squared splittings between the quasidegenerate states, while the off-diagonal elements proportional to ε contribute only to the active-plus-sterile mixing matrix.

The 6×6 neutrino mixing matrix is

$$\begin{aligned} V &= \begin{pmatrix} V_{e1} & V_{e2} & V_{e3} & V_{e1'} & V_{e2'} & V_{e3'} \\ V_{\mu 1} & V_{\mu 2} & V_{\mu 3} & V_{\mu 1'} & V_{\mu 2'} & V_{\mu 3'} \\ V_{\tau 1} & V_{\tau 2} & V_{\tau 3} & V_{\tau 1'} & V_{\tau 2'} & V_{\tau 3'} \\ V_{s_1 1} & V_{s_1 2} & V_{s_1 3} & V_{s_1 1'} & V_{s_1 2'} & V_{s_1 3'} \\ V_{s_2 1} & V_{s_2 2} & V_{s_2 3} & V_{s_2 1'} & V_{s_2 2'} & V_{s_2 3'} \\ V_{s_3 1} & V_{s_3 2} & V_{s_3 3} & V_{s_3 1'} & V_{s_3 2'} & V_{s_3 3'} \end{pmatrix} \\ &= \frac{1}{\sqrt{2}} \begin{pmatrix} 1_3 & -\delta \\ \delta^\dagger & 1_3 \end{pmatrix} \begin{pmatrix} U & -U \\ 1_3 & 1_3 \end{pmatrix}, \end{aligned} \qquad (2.9)$$

$$= \frac{1}{\sqrt{2}} \begin{pmatrix} U(1_3 - \frac{\epsilon^D}{2} - \varepsilon) & -U(1_3 + \frac{\epsilon^D}{2} + \varepsilon) \\ 1_3 + \frac{\epsilon^D}{2} - \varepsilon & 1_3 - \frac{\epsilon^D}{2} + \varepsilon \end{pmatrix}, \quad (2.10)$$

where we define the weak eigenstates as ν_α, $\alpha = e, \mu, \tau$, s_1, s_2, s_3 and the mass eigenstates as ν_i, $i = 1, 2, 3, 1', 2', 3'$. In the Dirac limit $\epsilon_m \to 0$, $V_{\alpha i} = -V_{\alpha i'} = U_{\alpha i}/\sqrt{2}$ ($\alpha = e, \mu, \tau$, $i = 1, 2, 3$) and $m_i = -m'_i$ ($i = 1, 2, 3$). We will order our states in the "usual" way [19]: $m_1^2 < m_2^2 < m_3^2$, $m_{1'}^2 < m_{2'}^2 < m_{3'}^2$ ($m_3^2 < m_1^2 < m_2^2$, $m_{3'}^2 < m_{1'}^2 < m_{2'}^2$) in the case of a normal (inverted) mass hierarchy. We assume the ϵ^D parameters small enough that the same mass hierarchy applies for the primed and unprimed eigenmasses. More specifically, $|m_i^2 - m_{i'}^2| \ll m_i^2$ for all $i = 1, 2, 3$.

In the next section we will concentrate on two subsets of the six neutrino mixing scenario: the case of two active and one right-handed neutrino, and the case of two active and two right-handed neutrinos. These will be described in more detail below and should serve as more concrete pedagogical examples.

In the case of two active (ν_e and ν_a, a linear combination of ν_μ and ν_τ) and one sterile neutrino ν_s, the 3×3 neutrino mass matrix can be written as

$$M_\nu = \begin{pmatrix} 0 & 0 & m\sin\theta \\ 0 & 0 & m\cos\theta \\ m\sin\theta & m\cos\theta & \epsilon_m \end{pmatrix}, \quad (2.11)$$

where $\epsilon_m \equiv m\epsilon$ is the Majorana mass of the right-handed neutrino. In the limit $\epsilon \ll 1$ (and ignoring the case when θ is very close to 0 or $\pi/2$), and assuming all parameters are real,

$$V^T M_\nu V = \begin{pmatrix} 0 & 0 & 0 \\ 0 & m(1 + \frac{\epsilon}{2}) & 0 \\ 0 & 0 & -m(1 - \frac{\epsilon}{2}) \end{pmatrix}, \quad (2.12)$$

where

$$V = \begin{pmatrix} V_{e1} & V_{e2} & V_{e2'} \\ V_{a1} & V_{a2} & V_{a2'} \\ V_{s1} & V_{s2} & V_{s2'} \end{pmatrix}$$

$$= \begin{pmatrix} \cos\theta & \frac{\sin\theta}{\sqrt{2}}(1 - \frac{\epsilon}{4}) & -\frac{\sin\theta}{\sqrt{2}}(1 + \frac{\epsilon}{4}) \\ -\sin\theta & \frac{\cos\theta}{\sqrt{2}}(1 - \frac{\epsilon}{4}) & -\frac{\cos\theta}{\sqrt{2}}(1 + \frac{\epsilon}{4}) \\ 0 & \frac{1}{\sqrt{2}}(1 + \frac{\epsilon}{4}) & \frac{1}{\sqrt{2}}(1 - \frac{\epsilon}{4}) \end{pmatrix}. \quad (2.13)$$

This system is described by three neutrino mass eigenstates: a massless one, ν_1, which is a linear combination of ν_e and ν_a, and two massive ones, $\nu_{2,2'}$, which are almost

degenerate in mass squared in the limit $\epsilon \ll 1$: $m_{2,2'}^2 \simeq m^2(1 \pm \epsilon)$, $m_2^2 - m_{2'}^2 = 2m^2\epsilon$. In a vacuum, the survival probability of electron neutrinos P_{ee} with energy E after a distance L has been traversed is

$$1 - P_{ee} = \frac{\sin^2 2\theta}{2}\left(1 - \frac{\epsilon}{2}\right)\sin^2\left(\frac{m^2(1 + \epsilon)L}{4E}\right)$$
$$+ \frac{\sin^2 2\theta}{2}\left(1 + \frac{\epsilon}{2}\right)\sin^2\left(\frac{m^2(1 - \epsilon)L}{4E}\right)$$
$$+ \sin^4\theta\sin^2\left(\frac{2m^2\epsilon L}{4E}\right),$$
$$= \sin^2 2\theta\sin^2\left(\frac{m^2 L}{4E}\right) + \mathcal{O}(\epsilon^2). \quad (2.14)$$

On the other hand, the oscillation probabilities of active neutrinos into sterile neutrinos are

$$P_{es} = \sin^2\theta\sin^2\left(\frac{2m^2\epsilon L}{4E}\right), \quad (2.15)$$

$$P_{as} = \cos^2\theta\sin^2\left(\frac{2m^2\epsilon L}{4E}\right). \quad (2.16)$$

Equation (2.14) agrees, of course, with the well-known two-neutrino oscillation probability in a vacuum in the limit $\epsilon \ll 1$. On the other hand, in the very long distance limit, $2m^2\epsilon L \sim E$, the oscillation due to the small mass-squared splitting can be observed on top of the averaged-out "active–active" oscillations,

$$\lim_{L \gg E/m^2} (1 - P_{ee}) = \frac{\sin^2 2\theta}{2} + \sin^4\theta\sin^2\left(\frac{2m^2\epsilon L}{4E}\right). \quad (2.17)$$

In the case of two active (ν_e and ν_a, a linear combination of ν_μ and ν_τ) and two sterile neutrinos ν_{s_1} and ν_{s_2}, the 4×4 neutrino mass matrix can be expressed as follows, assuming all parameters are real:

$$M_\nu = \begin{pmatrix} 0 & 0 & m_1\cos\theta & m_2\sin\theta \\ 0 & 0 & -m_1\sin\theta & m_2\cos\theta \\ m_1\cos\theta & -m_1\sin\theta & \epsilon_{m1} & \epsilon_{m3} \\ m_2\sin\theta & m_2\cos\theta & \epsilon_{m3} & \epsilon_{m2} \end{pmatrix}. \quad (2.18)$$

For concreteness, we allow $\theta \in [0, \pi/2]$ and define $m_2^2 > m_1^2$. In this case, reexpressing $\epsilon_{m1} = m_1\epsilon_1$, $\epsilon_{m2} = m_2\epsilon_2$, $\epsilon_{m3} = [(m_2^2 - m_1^2)/m_2]\epsilon_3$, and assuming all $\epsilon_i \ll 1$ and θ not too close to 0 or $\pi/2$,

$$V^T M_\nu V = \begin{pmatrix} m_1(1 + \frac{\epsilon_1}{2}) & 0 & 0 & 0 \\ 0 & m_2(1 + \frac{\epsilon_2}{2}) & 0 & 0 \\ 0 & 0 & -m_1(1 - \frac{\epsilon_1}{2}) & 0 \\ 0 & 0 & 0 & -m_2(1 - \frac{\epsilon_2}{2}) \end{pmatrix}, \quad (2.19)$$

where

$$V = \begin{pmatrix} V_{e1} & V_{e1'} & V_{e2} & V_{e2'} \\ V_{a1} & V_{a1'} & V_{a2} & V_{a2'} \\ V_{s_11} & V_{s_11'} & V_{s_12} & V_{s_12'} \\ V_{s_21} & V_{s_21'} & V_{s_22} & V_{s_22'} \end{pmatrix}$$

$$= \frac{1}{\sqrt{2}} \begin{pmatrix} U_2(1-E)_2 & -U_2(1+E)_2 \\ (1+E)_2^\dagger & (1-E)_2^\dagger \end{pmatrix}, \qquad (2.20)$$

and the 2×2 matrices

$$U_2 = \begin{pmatrix} \cos\theta & \sin\theta \\ -\sin\theta & \cos\theta \end{pmatrix},$$

$$(1 \pm E)_2 = \begin{pmatrix} 1 \pm \frac{\epsilon_1}{4} & \mp \frac{m_1}{m_2}\epsilon_3 \\ \pm\epsilon_3 & 1 \pm \frac{\epsilon_2}{4} \end{pmatrix}. \qquad (2.21)$$

This system is characterized by four mass eigenstates ν_1, ν_2, $\nu_{1'}$, $\nu_{2'}$ which are pairwise quasidegenerate in mass

squared. Oscillations are described by six distinct oscillation frequencies: $\Delta m^2_{12} = m^2_2 - m^2_1 + m^2_2\epsilon_2 - m^2_1\epsilon_1$, $\Delta m^2_{1'2} = m^2_2 - m^2_1 + m^2_2\epsilon_2 + m^2_1\epsilon_1$, $\Delta m^2_{12'} = m^2_2 - m^2_1 - m^2_2\epsilon_2 - m^2_1\epsilon_1$, $\Delta m^2_{1'2'} = m^2_2 - m^2_1 - m^2_2\epsilon_2 + m^2_1\epsilon_1$, $\Delta m^2_{1'1} = 2m^2_1\epsilon_1$, and $\Delta m^2_{2'2} = 2m^2_2\epsilon_2$ (in the limit ϵ_1, $\epsilon_2 \ll 1$). It is convenient to also express the two small frequencies in terms of the elements of the Majorana mass matrix for the right-handed neutrinos: $\Delta m^2_{1'1} = 2m_1\epsilon_{m1}$, and $\Delta m^2_{2'2} = 2m_2\epsilon_{m2}$. If all elements of ϵ_m are of the same order of magnitude, one expects $\Delta m^2_{2'2} > \Delta m^2_{1'1}$ since $m^2_2 > m^2_1$.

In a vacuum, the survival probability of electron neutrinos P_{ee} with energy E after a distance L has been traversed is

$$1 - P_{ee} = \frac{\sin^2 2\theta}{4} \left[\left(1 - \frac{\epsilon_1}{2} - \frac{\epsilon_2}{2}\right)\sin^2\left(\frac{\Delta m^2_{12}L}{4E}\right) + \left(1 - \frac{\epsilon_1}{2} + \frac{\epsilon_2}{2}\right)\sin^2\left(\frac{\Delta m^2_{1'2}L}{4E}\right) + \left(1 + \frac{\epsilon_1}{2} - \frac{\epsilon_2}{2}\right)\sin^2\left(\frac{\Delta m^2_{12'}L}{4E}\right) \right.$$

$$+ \left(1 + \frac{\epsilon_1}{2} + \frac{\epsilon_2}{2}\right)\sin^2\left(\frac{\Delta m^2_{1'2'}L}{4E}\right) \right] + \epsilon_3 \frac{\sin 2\theta}{2m_2} \left\{ (\cos^2\theta m_1 - \sin^2\theta m_2) \cos\left(\frac{\Delta m^2_{12}L}{2E}\right) \right.$$

$$+ (\cos^2\theta m_1 + \sin^2\theta m_2) \cos\left(\frac{(\Delta m^2_{12} - \Delta m^2_{11'})L}{2E}\right) + (-\cos^2\theta m_1 + \sin^2\theta m_2) \cos\left(\frac{(\Delta m^2_{11'} - \Delta m^2_{12'})L}{2E}\right)$$

$$- (\cos^2\theta m_1 + \sin^2\theta m_2) \cos\left(\frac{\Delta m^2_{12'}L}{2E}\right) \right\} + \cos^4\theta \sin^2\left(\frac{\Delta m^2_{1'1}L}{4E}\right) + \sin^4\theta \sin^2\left(\frac{\Delta m^2_{2'2}L}{4E}\right), \qquad (2.22)$$

$$= \sin^2 2\theta \sin^2\left(\frac{(m^2_2 - m^2_1)L}{4E}\right) + \mathcal{O}(\epsilon^2). \qquad (2.23)$$

Above, $\mathcal{O}(\epsilon^2)$ indicates terms which are of order the product of two ϵ_i, $i = 1, 2, 3$ (ϵ_1^2, $\epsilon_1\epsilon_2$, etc.). It is trivial to note that, for small enough ϵ_1, ϵ_2, ϵ_3, the two-flavor vacuum oscillation expression is reproduced, as expected. Finally, in the very long baseline limit, assuming that the fast 12 (and $1'2$, $12'$, $1'2'$) oscillations average out,

$$\lim_{L \gg E/(m^2_2 - m^2_1)} (1 - P_{ee}) = \frac{\sin^2 2\theta}{2} + \cos^4\theta \sin^2\left(\frac{2m^2_1\epsilon_1 L}{4E}\right)$$

$$+ \sin^4\theta \sin^2\left(\frac{2m^2_2\epsilon_2 L}{4E}\right). \qquad (2.24)$$

Again as expected, in the very long baseline limit the electron neutrino survival probability is equal to the averaged out "active oscillation" effect, plus two long-wavelength components driven by the $1'1$ and $2'2$ mass-squared splittings. Two features are readily visible: One is that there is no dependency on the off-diagonal ϵ_3 parameter [this only appears as $\mathcal{O}(\epsilon^2)$ level corrections to the coefficients of the different terms in Eq. (2.24)]. The second is that, assuming $\cos^4\theta \sim \sin^4\theta$, we expect to be more sensitive to ϵ_2 than ϵ_1, as the $2'2$ oscillations "turn on" before the $1'1$-oscillations (remember $m^2_2 > m^2_1$).

III. CURRENT CONSTRAINTS

If one assumes that there are three right-handed neutrinos with Majorana masses much smaller than the Dirac neutrino masses that govern "active" neutrino oscillations, current experimental data can be used to constrain the right-handed neutrino Majorana mass matrix ϵ_m. There are, however, too many free parameters in ϵ_m, and the individual upper bound on each of these is not very illuminating and outside the aspirations of this work. Such a bound will also depend on aspects of neutrino masses and mixing that are currently unknown, including the neutrino mass hierarchy and $|U_{e3}|^2$. We are, however, interested in asking what is the constraint on ϵ_m assuming that all its elements are of the same order of magnitude. Hence we will concentrate on the current experimental upper bound on the element of ϵ_m that is best constrained. This will become clear in the following paragraphs.

Consider that the three neutrino mass eigenstates ν_1, ν_2, ν_3 identified experimentally [19] are in reality split into, say,[3] six states ν_1, ν_2, ν_3, $\nu_{1'}$, $\nu_{2'}$, $\nu_{3'}$. As discussed in the

_____

[3]The current data are also consistent with two right-handed neutrinos. In this case, the massless neutrino mass eigenstate is not split, and also does not contain a sterile neutrino component. This is identical to the $2 + 1$ case [Eq. (2.11)] discussed in the previous section.

previous section, these splittings will manifest themselves via new, very long wavelength oscillations characterized by the $\Delta m_{i'i}^2$ mass-squared differences ($i = 1, 2, 3$). These, on the other hand, are proportional to $\epsilon_{m_{ii}} m_i$, and the largest new mass-squared splitting is associated to the $\epsilon_{m_{ii}}$ value associated to the largest m_i^2. In turn, the largest m_i^2 value depends on the neutrino mass hierarchy. In the case of an inverted mass hierarchy, $m_2^2 > m_1^2 \gtrsim 2 \times 10^{-3}$ eV^2 is the largest m_i^2. On the other hand, if the hierarchy is normal, $m_3^2 \gtrsim 2 \times 10^{-3}$ eV^2 is the largest m_i^2 while $m_2^2 > m_1^2$ and $m_2^2 \gtrsim 8 \times 10^{-5}$ eV^2.

Ignoring $|U_{e3}|$-driven effects, $\Delta m_{3'3}^2$ is best constrained by the disappearance of muon-type neutrinos and antineutrinos produced in the atmosphere. We estimate that these experiments are sensitive to ϵ_m values that lead to new oscillation lengths which are not much larger than the diameter of the earth, or

$$L_{\mathrm{osc}}^{3'3} = \frac{1}{\epsilon_3} \left(\frac{10^{-3} \ \mathrm{eV}^2}{m_3^2}\right)\left(\frac{E}{100 \ \mathrm{MeV}}\right) \times 10^2 \ \mathrm{km} \lesssim 10^4 \ \mathrm{km}. \tag{3.1}$$

Hence atmospheric experiments can "see" ϵ_3 values larger than around 10^{-2}. This, in turn, translates into a sensitivity to ϵ_m elements of order $\epsilon_m \gtrsim \sqrt{10^{-3}} \times 10^{-2}$ eV. A more detailed estimate can be extracted from the analyses performed in [20]. In more detail, atmospheric data constrain the new mass-squared difference to be less than about 10^{-4} eV^2. In the case of a normal mass hierarchy, this translates into $4\epsilon_3 \times 10^{-3}$ eV$^2 \lesssim 10^{-4}$ eV^2 or $\epsilon_3 \lesssim 0.03$ and $\epsilon_m \lesssim 0.001$ eV. The estimate above was made for $m_3^2 = 2 \times 10^{-3}$ eV^2.

$\Delta m_{2'2}^2$ (and $\Delta m_{1'1}^2$) is best constrained by solar neutrino experiments. Ultimately, one is sensitive to oscillation lengths of order the earth–sun distance (1 A.U. = 149.6 × 10^6 km). Naively, the sensitivity to ϵ_2 and ϵ_1 can be estimated from

$$L_{\mathrm{osc}}^{1'1,2'2} = \frac{10^{-7}}{\epsilon_{1,2}} \left(\frac{8 \times 10^{-5} \ \mathrm{eV}^2}{m_{1,2}^2}\right)\left(\frac{E}{1 \ \mathrm{MeV}}\right) \times 1 \ \mathrm{A.U.}$$
$$\lesssim 1 \ \mathrm{A.U.}, \tag{3.2}$$

which translates into $\epsilon_{1,2} \gtrsim 10^{-7}$ if both m_1 and m_2 are of the same order. This translates into a sensitivity to ϵ_m elements of order $\epsilon_m \gtrsim \sqrt{8 \times 10^{-5}} \times 10^{-7}$ eV. Both sensitivity estimates ($\epsilon_3 \gtrsim 10^{-2}$ and $\epsilon_{1,2} \gtrsim 10^{-7}$) are quoted assuming the Dirac neutrino mass hierarchy is normal. In the case of an inverted hierarchy the sensitivity of atmospheric neutrino experiments to ϵ_3 is markedly worse, while that of solar neutrino experiments to $\epsilon_{1,2}$ is markedly better. Finally, if the Dirac neutrino masses are quasidegenerate and much larger in magnitude than $\sqrt{\Delta m_{13}^2} \sim 0.05$ eV (the atmospheric mass-squared difference), the

sensitivity to all ϵ_i is expected to be better than estimated above.

In conclusion, constraints on $\epsilon_{1,2}$ from solar neutrino data provide, by far, the best bound on a given ϵ_m element, regardless of the neutrino mass hierarchy. Therefore, we will concentrate on the effect of the seesaw right-handed neutrinos in solar oscillations. We will further assume $|U_{e3}|$ is small enough so that ν_3 and $\nu_{3'}$ related effects in experiments with electron neutrinos in the initial state are negligible and will concentrate on an effective system consisting of the electron neutrino, the linear combination ν_a of ν_μ and ν_τ orthogonal to the one in $\nu_{3,3'}$, and either one or two sterile states.

A. Oscillation of solar neutrinos, 2 + 1 case

We first discuss the case of only one right-handed neutrino, Eq. (2.11), where $m_1 \equiv 0$. The 2 + 1 scenario captures most of the physics of the 2 + 2 case, which will be discussed in the next subsection, and contains all the relevant information in the limit $m_1 \ll m_2$. In the 2 + 1 case, the effect of right-handed neutrinos is entirely captured by one dimensionless parameter ϵ. Furthermore, the neutrino mass responsible for the oscillation of solar neutrinos and reactor antineutrinos at KamLAND is uniquely determined: $m^2 = (7.59 \pm 0.21) \times 10^{-5}$ eV^2 [21] from KamLAND data. We will show that ϵ is constrained to be small enough that this measurement is not affected by the presence of the sterile neutrino [see Eq. (2.14)]. The other parameter in M_ν, the mixing angle θ, is mostly determined by solar data, more specifically those from SNO and Super-Kamiokande. We will argue later that the impact of ϵ_m on the determination of θ is not significant.

We first briefly discuss how neutrinos produced in the core of the sun propagate towards the surface of the sun and then to a detector on earth, and calculate the relevant transition probabilities. We hence construct the effective Hamiltonian H in the flavor basis in the presence of the matter [22]:

$$H = \frac{M_\nu^\dagger M_\nu}{2E} + \begin{pmatrix} A & & \\ & 0 & \\ & & 0 \end{pmatrix}$$
$$= \begin{pmatrix} A + \frac{m^2 \sin^2\theta}{2E} & \frac{m^2 \sin\theta\cos\theta}{2E} & \frac{m^2 \epsilon \sin\theta}{2E} \\ \frac{m^2 \sin\theta\cos\theta}{2E} & \frac{m^2 \cos^2\theta}{2E} & \frac{m^2 \epsilon \cos\theta}{2E} \\ \frac{m^2 \epsilon \sin\theta}{2E} & \frac{m^2 \epsilon \cos\theta}{2E} & \frac{m^2(1+\epsilon^2)}{2E} \end{pmatrix}, \tag{3.3}$$

where $A = \sqrt{2} G_F N_e$ is the matter potential due to electrons, G_F is the Fermi constant, N_e is the position-dependent electron number density, and E is the neutrino energy. In principle, we should also consider the effect of neutral current interactions due to the presence of neutrons. This contribution, however, is expected to be negligible in the sun given that it consists mostly of hydrogen (hence "neutron-poor"), and the proton and electron neutral current contributions cancel out. Under this approximation,

analytical solutions for the transition probability can be easily obtained as long as N_e is a simple enough function of the neutrino position.

It is easy to understand how an electron neutrino produced in the sun's core propagates first to the sun's surface and later to the detectors on earth. It is illustrative to discuss what happens in the $\epsilon \to 0$ limit. In this case, one of the eigenvectors of H [Eq. (3.3)], with eigenvalue $m^2/2E$, is independent of A and is purely sterile. In the basis defined by Eq. (2.13) it is neither ν_2 nor $\nu_{2'}$ but $1/\sqrt{2}(\nu_2 + \nu_{2'})$.[4] The other two states are purely active and can be obtained by diagonalizing the familiar matter-affected two-by-two neutrino propagation Hamiltonian. For m^2 values of interest, electron neutrinos are produced in the sun's core and propagate adiabatically, exiting the sun as an incoherent mixture of ν_1 and $1/\sqrt{2}(\nu_2 - \nu_{2'})$ with probabilities $\cos^2\theta_M$ and $\sin^2\theta_M$, respectively, where the matter mixing angle is defined at the production region by the familiar expression

$$
\begin{aligned}
\sin 2\theta_M &= \frac{\Delta \sin 2\theta}{\sqrt{(\Delta \cos 2\theta - A)^2 + \Delta^2 \sin^2 2\theta}}, \\
\cos 2\theta_M &= \frac{\Delta \cos 2\theta - A}{\sqrt{(\Delta \cos 2\theta - A)^2 + \Delta^2 \sin^2 2\theta}},
\end{aligned}
\tag{3.4}
$$

where $\Delta \equiv m^2/2E$. In this case, P_{ee} at the surface of the sun (or the earth) is given by

$$
\begin{aligned}
\lim_{\epsilon \to 0} P_{ee}^{\text{solar}} &= \cos^2\theta_M |V_{e1}|^2 + \frac{\sin^2\theta_M}{2} |V_{e2} - V_{e2'}|^2 \\
&= \cos^2\theta_M \cos^2\theta + \sin^2\theta_M \sin^2\theta,
\end{aligned}
\tag{3.5}
$$

which is the familiar result for solar neutrino oscillations in the so-called large mixing angle (LMA) region.

Figure 1 depicts the evolution of the instantaneous eigenvalues of H inside the sun, as a function of R, the distance from the sun's center, for $\epsilon \neq 0$. For illustrative purposes we choose, for the Hamiltonian parameters, $E = 5$ MeV, $m^2 = 8.1 \times 10^{-5}$ eV^2, $\sin^2\theta = 0.3$, $\epsilon = 3 \times 10^{-1}$. The LMA Mikheyev-Smirnov-Wolfenstein (MSW) resonance (between the largest eigenvalue and the smallest one) can be readily identified (at $R \sim 0.1$). One can also see the impact of $\epsilon \neq 0$: the top two eigenvalues are split for all values of R. Furthermore, there is another "resonance" [23] due to the small but nonzero ϵ at larger R between the two heaviest Hamiltonian eigenstates. This will be discussed momentarily.

Assuming that the crossing of the LMA MSW resonance is adiabatic and that $\epsilon \ll 1$, the electron neutrino survival probability can be written as

----

[4]In the limit $\epsilon \to 0$, ν_2 and $\nu_{2'}$ have the same mass-squared and hence any linear combination of them is an eigenstate of the propagation Hamiltonian in a vacuum.
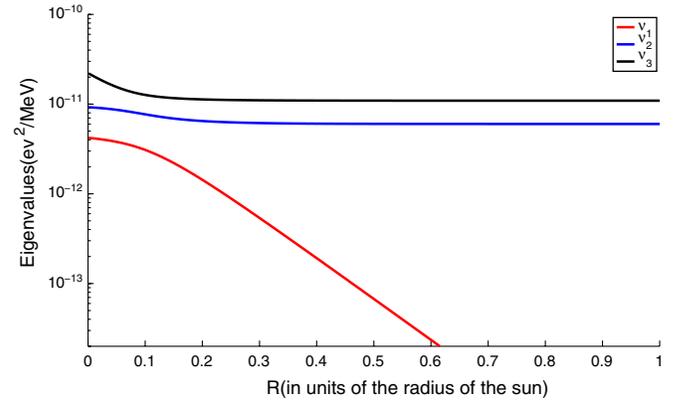

FIG. 1 (color online). The evolution of instantaneous eigenvalues of the Hamiltonian inside the sun in the $2 + 1$ scenario, Eq. (3.3), for $E = 5$ MeV, $m^2 = 8.1 \times 10^{-5}$ eV^2, $\sin^2\theta = 0.3$, $\epsilon = 3 \times 10^{-1}$.

$$
\begin{aligned}
P_{ee} = \Bigg| (1\,0\,0)V &\begin{pmatrix} \exp(-i\phi_1') & 0 & 0 \\ 0 & \exp(-i\phi_2') & 0 \\ 0 & 0 & \exp(-i\phi_3') \end{pmatrix} \\
\times &\begin{pmatrix} 1 & 0 & 0 \\ 0 & \sqrt{1-P_c} & -\sqrt{P_c} \\ 0 & \sqrt{P_c} & \sqrt{1-P_c} \end{pmatrix} \\
\times &\begin{pmatrix} \exp(-i\phi_1) & 0 & 0 \\ 0 & \exp(-i\phi_2) & 0 \\ 0 & 0 & \exp(-i\phi_3) \end{pmatrix} V_{\text{mat}}^\dagger \begin{pmatrix} 1 \\ 0 \\ 0 \end{pmatrix} \Bigg|^2,
\end{aligned}
\tag{3.6}
$$

where [24]

$$
P_c = \frac{e^{-\gamma |V_{s2}|^2} - e^{-\gamma}}{1 - e^{-\gamma}},
$$

$$
\gamma \simeq 9.8 \left(\frac{\epsilon}{10^{-4}} \right) \left(\frac{m^2}{8 \times 10^{-5}\,\text{eV}^2} \right) \left(\frac{0.862\,\text{MeV}}{E} \right),
\tag{3.7}
$$

V is given by Eq. (2.13), and V_{mat} is the unitary matrix that diagonalizes Eq. (3.3) at the production point. Equation (3.6) can be understood as follows. The electron neutrino is first expressed in the basis of the Hamiltonian at the production point. It then propagates adiabatically (each component acquiring a phase factor ϕ_i, $i = 1, 2, 3$) until it gets to the location of the resonance between the two "heaviest" instantaneous Hamiltonian eigenstates. Around that point, the unitary evolution is characterized by the matrix containing P_c, which is the crossing probability between the two Hamiltonian eigenstates. Finally, it propagates from that point until it gets to the earth (each component acquiring a phase factor ϕ_i', $i = 1, 2, 3$), where we compute the probability that this state is an electron neutrino. For a similar discussion of P_{ee} in the presence of

a new small mass-squared difference, see, for example, [20].

We can estimate P_{ee} for $\epsilon \gtrsim 10^{-3}$ when P_c in Eq. (3.7) vanishes to a very good approximation for all neutrino energies below 10 MeV. If we consider the case $A \gg \Delta$ in the production region (this is an excellent approximation in the upper energy range of the ^{8}B solar neutrino spectrum), P_{ee} is very easy to compute since the electron neutrino is a Hamiltonian eigenstate at birth (corresponding to the heaviest Hamiltonian eigenstate) and the entire evolution of the state inside the sun is adiabatic. In summary, the electron neutrino exits the sun as the heaviest neutrino mass eigenstate, which we will assume to be ν_2 (which is the case for ϵ positive) and

$$P_{ee} = |V_{e2}|^2 = \frac{\sin^2\theta}{2}\left(1 - \frac{\epsilon}{2}\right), \qquad (3.8)$$

$$P_{ea} = |V_{\mu 2}|^2 = \frac{\cos^2\theta}{2}\left(1 - \frac{\epsilon}{2}\right), \qquad (3.9)$$

$$P_{es} = |V_{s2}|^2 = \frac{1}{2}\left(1 + \frac{\epsilon}{2}\right). \qquad (3.10)$$

It is easy to see that under these circumstances there is no value of θ that provides a good fit to the solar neutrino data, as we will discuss in more detail in Sec. III C.

On the other hand, in the limit $\epsilon \ll 10^{-3}$, it is sufficient to keep only the leading order ($\epsilon \to 0$) limit of V_{mat}. In more detail,

$$V_{\text{mat}}^\dagger \begin{pmatrix} 1 \\ 0 \\ 0 \end{pmatrix} = \begin{pmatrix} \cos\theta_M \\ \sin\theta_M \\ 0 \end{pmatrix} + \mathcal{O}(\epsilon), \qquad (3.11)$$

where θ_M is defined in Eq. (3.4). At the surface of the sun, after integrating over the neutrino production region, the electron neutrino is an incoherent mixture of ν_1 (with probability $\cos^2\theta_M$) and $\sqrt{1 - P_c}\nu_2 - \sqrt{P_c}\nu_{2'}$[5] (with probability $\sin^2\theta_M$). The latter may undergo vacuum oscillations on its way between the sun's surface and the earth with an oscillation probability given by

$$P(\sqrt{1 - P_c}\nu_2 - \sqrt{P_c}\nu_{2'} \to \nu_e)$$

$$= \left| V_{e2}\sqrt{1 - P_c} - V_{e2'}\sqrt{P_c}\exp\left[-i\frac{2m^2\epsilon L}{2E}\right]\right|^2,$$

$$= \frac{\sin^2\theta}{2}\left[1 + 2\sqrt{P_c(1 - P_c)}\cos\left(\frac{2m^2\epsilon L}{2E}\right)\right]. \qquad (3.12)$$

Combining all the information above,

_____

[5]An irrelevant relative phase factor between ν_2 and $\nu_{2'}$ has been omitted.

$$P_{ee} = \cos^2\theta_M\cos^2\theta + \sin^2\theta_M\frac{\sin^2\theta}{2}\left[1 + 2\sqrt{P_c(1 - P_c)}\right.$$
$$\left. \times \cos\left(\frac{2m^2\epsilon L}{2E}\right)\right],$$

$$P_{ea} = \cos^2\theta_M\sin^2\theta + \sin^2\theta_M\frac{\cos^2\theta}{2}\left[1 + 2\sqrt{P_c(1 - P_c)}\right.$$
$$\left. \times \cos\left(\frac{2m^2\epsilon L}{2E}\right)\right],$$

$$P_{es} = \sin^2\theta_M\frac{1}{2}\left[1 - 2\sqrt{P_c(1 - P_c)}\cos\left(\frac{2m^2\epsilon L}{2E}\right)\right]. \qquad (3.13)$$

Figure 2 depicts $P_{e\zeta}$ $\zeta = e, a, s$ for solar neutrinos as a function of energy for $m^2 = 7.6 \times 10^{-5}$ eV^2, $\sin^2\theta = 0.31$, and two different values of $\epsilon = 1 \times 10^{-7}$ and $\epsilon = 5 \times 10^{-8}$. In order to compute $P_{e\zeta}$, we integrate over the neutrino production region in the sun's core, taking into account that θ_M depends on N_e at the production point. For high-energy solar neutrinos P_{es} is small and P_{ee} is very similar to the standard LMA solution to the solar neutrino puzzle. For low-energy solar neutrinos, the oscillatory pattern becomes more pronounced and P_{es} becomes significantly nonzero. As already briefly discussed, for much larger values of ϵ, $P_c \to 0$ and $P_{es} \simeq \sin^2\theta_M/2$ is roughly equal to one-half for high-energy solar neutrinos. On the flip side, for smaller values of ϵ, $P_c \to 1/2$ and the argument of the cosine in Eq. (3.13) is vanishingly small. In this case, as already discussed, sterile neutrino effects disap-
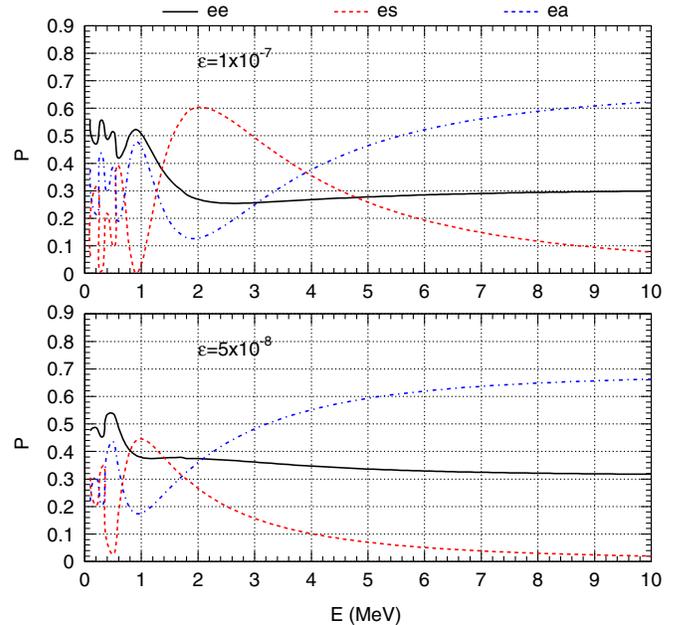

FIG. 2 (color online). $P_{e\zeta}$ for solar neutrinos at the surface of the earth, $\zeta = e, a, s$, as a function of neutrino energy for $m^2 = 7.6 \times 10^{-5}$ eV^2, $\sin^2\theta = 0.31$. Top: $\epsilon = 1 \times 10^{-7}$. Bottom: $\epsilon = 5 \times 10^{-8}$.

pear and we recover the standard LMA solution to the solar neutrino puzzle.

B. Oscillation of solar neutrinos, 2 + 2 case

It is straightforward to generalize the results obtained in the previous subsection to the case of two active (ν_e and ν_a) and two sterile neutrinos (ν_1 and ν_2). In this case, the Hamiltonian that governs neutrino oscillations in neutral hydrogen matter characterized by an electron number density N_e is

$$H = \frac{M_\nu^\dagger M_\nu}{2E} + \begin{pmatrix} A & & & \\ & 0 & & \\ & & 0 & \\ & & & 0 \end{pmatrix}$$

$$= \begin{pmatrix} U_2 & \\ & 1_2 \end{pmatrix}$$

$$\times \begin{pmatrix} A\cos^2\theta + \frac{m_1^2}{2E} & A\cos\theta\sin\theta & \frac{\epsilon_1 m_1^2}{2E} & \frac{\epsilon_3(\frac{\Delta m^2 m_1}{m_2})}{2E} \\ A\cos\theta\sin\theta & A\sin^2\theta + \frac{m_2^2}{2E} & \frac{\epsilon_3\Delta m^2}{2E} & \frac{\epsilon_2 m_2^2}{2E} \\ \frac{\epsilon_1 m_1^2}{2E} & \frac{\epsilon_3\Delta m^2}{2E} & \frac{m_1^2(1+\mathcal{O}(\epsilon^2))}{2E} & \mathcal{O}(\epsilon^2) \\ \frac{\epsilon_3(\frac{\Delta m^2 m_1}{m_2})}{2E} & \frac{\epsilon_2 m_2^2}{2E} & \mathcal{O}(\epsilon^2) & \frac{m_2^2(1+\mathcal{O}(\epsilon^2))}{2E} \end{pmatrix}$$

$$\times \begin{pmatrix} U_2^\dagger & \\ & 1_2 \end{pmatrix}.$$

$$(3.14)$$

Here, M_ν is given by Eq. (2.18), while U_2 and 1_2 are defined in Eq. (2.21). We define $\Delta m^2 \equiv m_2^2 - m_1^2$. Note that a diag($U_2$, 1_2) rotation expresses the Hamiltonian in an active–sterile-mass-squared basis where the top two components consist of two mass-squared states that are mostly active, while the bottom two components consist of two mass-squared states that are mostly sterile. The Hamiltonian is block diagonal in this basis in the limit $\epsilon_{1,2,3} \to 0$. In this limit, of course, we are left with the standard MSW Hamiltonian for two active neutrino flavors.

Figure 3 depicts the evolution of the instantaneous eigenvalues of H inside the sun, as a function R, the distance from the sun's center, for $\epsilon_{1,2,3} \neq 0$. For illustrative purposes, we choose $E = 10$ MeV, $m_1^2 = 1 \times 10^{-6}$ eV², $m_2^2 = 8.2 \times 10^{-5}$ eV², $\sin^2\theta = 0.32$, $\epsilon_1 = 3 \times 10^{-1}$, $\epsilon_2 = 4 \times 10^{-1}$, and $\epsilon_{m3} = 10^{-3}$ eV for the Hamiltonian parameters. The LMA MSW resonance (between the largest eigenvalue and the smallest one) can be readily identified (at $R \sim 0.1$). One can also see the impact of $\epsilon_{1,2,3} \neq 0$: the top two and the bottom two eigenvalues are split for all values of R. Similar to the 2 + 1 case discussed in the previous subsection, there are two other resonances [23] due to the small but nonzero $\epsilon_{1,2,3}$ at larger R between the two largest and two smallest Hamiltonian eigenstates. From the Hamiltonian Eq. (3.14), it is easy to see that these are governed by the small parameters ϵ_1 (resonance be-
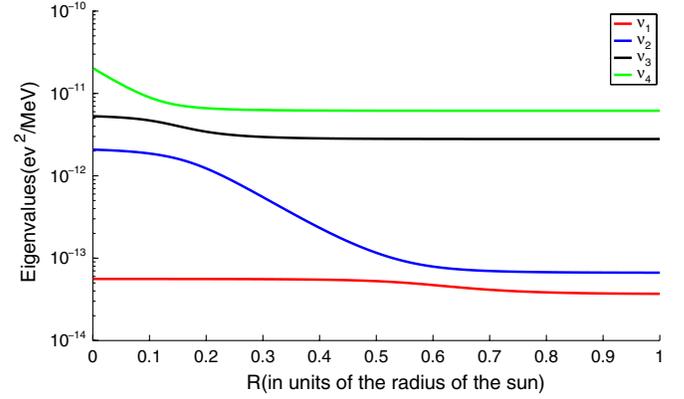

FIG. 3 (color online). The evolution of instantaneous eigenvalues of the Hamiltonian inside the sun in the 2 + 2 scenario, Eq. (3.14), for $E = 10$ MeV, $m_1^2 = 1 \times 10^{-6}$ eV², $m_2^2 = 8.2 \times 10^{-5}$ eV², $\sin^2\theta = 0.32$, $\epsilon_1 = 3 \times 10^{-1}$, $\epsilon_2 = 4 \times 10^{-1}$, and $\epsilon_{m3} = 10^{-3}$ eV.

tween the two lightest states) and ϵ_2 (resonance between the two heaviest states). ϵ_3 connects the *heaviest* active state to the *lightest* "sterile" state (and vice versa) and, for physically interesting values of the neutrino oscillation parameters, its effects are not visible.

As in the 2 + 1 case, $\Delta m^2 = (7.59 \pm 0.21) \times 10^{-5}$ eV² is fixed by the results of the KamLAND experiment, and $\sin^2\theta$ is constrained to be large. In this case, electron neutrino production in the sun's core and subsequent propagation can be described as follows. The electron neutrino is produced as an incoherent superposition of the two mostly active states [this is true as long as $A \gg \epsilon_{1,3}m_1^2/(2E)$ for all values of E of interest]. The two components then evolve adiabatically until they hit the resonances governed by ϵ_1 and ϵ_2. Hence the electron neutrino exits the sun as an incoherent mixture of $\sqrt{1 - P_{c1}}\nu_1 - \sqrt{P_{c1}}\nu_{1'}$ (with probability $\cos^2\theta_M$) and $\sqrt{1 - P_{c2}}\nu_2 - \sqrt{P_{c2}}\nu_{2'}$ (with probability $\sin^2\theta_M$).[6] Here, θ_M is defined by Eq. (3.4). The crossing probabilities are given by

$$P_{c,i} = \frac{e^{-\gamma_i|V_{s_ii}|^2} - e^{-\gamma_i}}{1 - e^{-\gamma}},$$

$$\gamma_i \simeq 9.8\left(\frac{\epsilon_i}{10^{-4}}\right)\left(\frac{m_i^2}{8 \times 10^{-5} \text{ eV}^2}\right)\left(\frac{0.862 \text{ MeV}}{E}\right),$$

$$i = 1, 2, \qquad (3.15)$$

where V_{s_ii} are given in Eq. (2.20). On their way to the surface of the earth, both of these states can undergo vacuum oscillations driven by the mass-squared differences $2m_1^2\epsilon_1$ and $2m_2^2\epsilon_2$ [see Eq. (2.24)]. One can write

---

[6]Relative phases between ν_i and $\nu_{i'}$, $i = 1, 2$ have been ignored as neither of them is observable in practice.

$$P_{ee} = \cos^2\theta_M \times P(\sqrt{1 - P_{c1}}\,\nu_1 - \sqrt{P_{c1}}\,\nu_{1'} \to \nu_e)$$
$$+ \sin^2\theta_M \times P(\sqrt{1 - P_{c2}}\,\nu_2 - \sqrt{P_{c2}}\,\nu_{2'} \to \nu_e), \quad (3.16)$$

where $P(\sqrt{1 - P_{c1}}\,\nu_1 - \sqrt{P_{c1}}\,\nu_{1'} \to \nu_e)$ is given by Eq. (3.12) with P_c, m, ϵ replaced by P_{c1}, m_1, ϵ_1, respec-

tively, and $U_{e2,e2'}$ replaced by $U_{e1,e1'}$. Similarly, $P(\sqrt{1 - P_{c2}}\,\nu_2 - \sqrt{P_{c2}}\,\nu_{2'} \to \nu_e)$ is given by Eq. (3.12) with P_c, m, ϵ replaced by P_{c2}, m_2, ϵ_2, respectively. After the dust settles,

$$P_{ee} = \cos^2\theta_M \frac{\cos^2\theta}{2}\left[1 + 2\sqrt{P_{c1}(1 - P_{c1})}\cos\left(\frac{m_1^2\epsilon_1 L}{E}\right)\right] + \sin^2\theta_M \frac{\sin^2\theta}{2}\left[1 + 2\sqrt{P_{c2}(1 - P_{c2})}\cos\left(\frac{m_2^2\epsilon_2 L}{E}\right)\right],$$

$$P_{ea} = \cos^2\theta_M \frac{\sin^2\theta}{2}\left[1 + 2\sqrt{P_{c1}(1 - P_{c1})}\cos\left(\frac{m_1^2\epsilon_1 L}{E}\right)\right] + \sin^2\theta_M \frac{\cos^2\theta}{2}\left[1 + 2\sqrt{P_{c2}(1 - P_{c2})}\cos\left(\frac{m_2^2\epsilon_2 L}{E}\right)\right], \quad (3.17)$$

$$P_{es} = \cos^2\theta_M \frac{1}{2}\left[1 - 2\sqrt{P_{c1}(1 - P_{c1})}\cos\left(\frac{m_1^2\epsilon_1 L}{E}\right)\right] + \sin^2\theta_M \frac{1}{2}\left[1 - 2\sqrt{P_{c2}(1 - P_{c2})}\cos\left(\frac{m_2^2\epsilon_2 L}{E}\right)\right],$$

where $P_{es} \equiv P_{es_1} + P_{es_2}$ and θ_M is given by Eq. (3.4). In all expressions above, we have assumed all $\epsilon_{1,2,3}$ much smaller than 1. This will be justified *a posteriori* (see Sec. III C) for ϵ_1 and ϵ_2, and we postulate that it is valid for ϵ_3. The impact of a "large" ϵ_3 is mostly felt in the diagonalization of H [Eq. (3.14)] in the production region, which we assumed is properly described only by the matter mixing angle θ_M [see Eq. (3.11)]. The bound one would obtain on ϵ_{m3} via these effects is much worse (by many orders of magnitude) than the bounds on ϵ_{m1} and ϵ_{m2} discussed in the next subsection. As explained earlier, we are interested in the most stringent bound on any element of ϵ_m and will not consider these ϵ_3 effects henceforth. On a related note, Eq. (3.17) does not depend on ϵ_3, similar to Eq. (2.24). For this reason we will not discuss ϵ_3 effects or bounds.

Figure 4 depicts $P_{e\zeta}$ for solar neutrinos at the surface of the earth, $\zeta = e, a, s$, as a function of neutrino energy for $m_1^2 = 1.0 \times 10^{-6}$ eV^2, $m_2^2 = 8.2 \times 10^{-5}$ eV^2, $\sin^2\theta = 0.31$, and $\epsilon_1 = 1 \times 10^{-6}$, plus two different values of $\epsilon_2 = 1 \times 10^{-9}$ and $\epsilon_2 = 1 \times 10^{-7}$. It is easy to see that dominant ϵ_1 effects are most visible for low-energy solar neutrinos, when $\cos^2\theta_M$ is significantly different from zero [Fig. 4 (top)]. On the other hand, dominant ϵ_2 effects are identical to the ones observed in the $2 + 1$ case, where ϵ_2 plays the role of ϵ. The main distinction is the fact that in the $2 + 1$ case m^2 was constrained by KamLAND, while in the $2 + 2$ case neither m_1^2 nor m_2^2 is strongly constrained by data, except through their difference: $m_2^2 - m_1^2 = 7.6 \times 10^{-5}$ eV^2. In the case when both ϵ_1 and ϵ_2 are non-negligible [Fig. 4 (bottom)], one can see that ϵ_2 effects are dominant for high-energy solar neutrinos (cf. Figure 2), while ϵ_1 and ϵ_2 effects "add up" for the low-energy solar neutrinos.

C. Constraints from experimental data

The flux of electron neutrinos from the sun has been measured, sometimes as a function of energy, by a variety of experiments and in a variety of ways. The flux of active

neutrinos from the sun has also been unambiguously measured for ^{8}B neutrinos. Here, we use recent data from [25–31] in order to constrain ϵ (in the $2 + 1$ case) and $\epsilon_{1,2}$ (in the $2 + 2$ case). In order to compute the expected event rates at the different experiments we use parameters from the BS05(OP) version of the standard solar model [32].

We do not attempt an exhaustive analysis of all neutrino data but instead concentrate on the features that most impact our results. We make use of the following observables. More details are provided in the Appendix.

(i) ϕ^{CC} (SNO), the integrate ^{8}B neutrino flux measured via $\nu_e + {}^2\text{H} \to e^- + p + p$ at SNO [25–27]. This observable is sensitive only to the electron neutrino component of the solar neutrino flux.
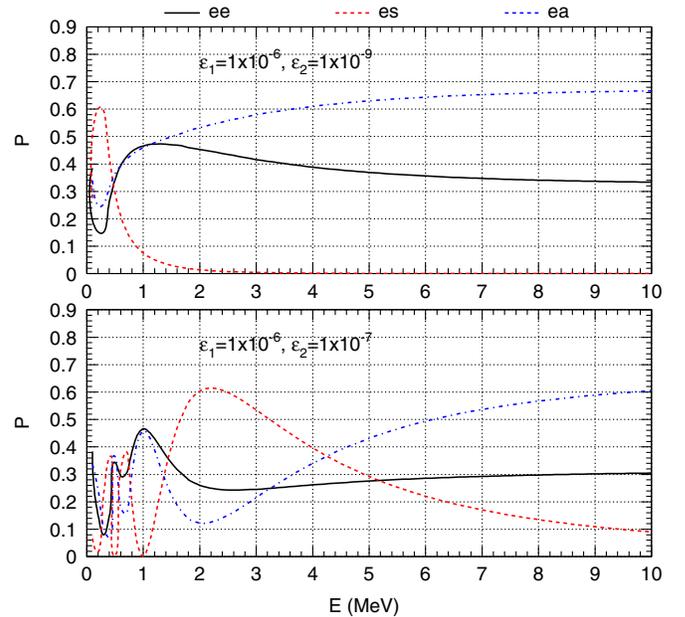

FIG. 4 (color online). $P_{e\zeta}$ for solar neutrinos at the surface of the earth, $\zeta = e, a, s$, as a function of neutrino energy for $m_1^2 = 1.0 \times 10^{-6}$ eV^2, $m_2^2 = 8.2 \times 10^{-5}$ eV^2, $\sin^2\theta = 0.31$. Top: $\epsilon_1 = 1 \times 10^{-6}$, $\epsilon_2 = 1 \times 10^{-9}$. Bottom: $\epsilon_1 = 1 \times 10^{-6}$, $\epsilon_2 = 1 \times 10^{-7}$.

(ii) ϕ^{NC} (SNO), the integrated ^{8}B neutrino flux measured via $\nu_{e,a} + {}^2\text{H} \rightarrow \nu_{e,a} + n + p$ at SNO [25–27]. This observable is sensitive to the active neutrino component of the solar neutrino flux.

(iii) ϕ^{ES} (SuperK), the ^{8}B neutrino flux measured via $\nu_{e,a} + e^- \rightarrow \nu_{e,a} + e^-$ at Super-Kamiokande [28] integrated over a handful of recoil electron energy bins. This observable is sensitive to the active neutrino component of the solar neutrino flux. The cross section for muon or tau-type neutrino–electron scattering is about 0.16 times that of electron-type neutrino–electron scattering when integrated over the ^{8}B neutrino energy spectrum. SNO also has data on neutrino–electron elastic scattering (also included), but with significantly fewer statistics than Super-Kamiokande.

(iv) ϕ^{ES} (Borexino), the ^{7}Be neutrino flux[7] measured via $\nu_{e,a} + e^- \rightarrow \nu_{e,a} + e^-$ at Borexino [31]. This observable is sensitive to the active neutrino component of the solar neutrino flux. The cross section for muon or tau-type neutrino–electron scattering is about 0.21 times that of electron-type neutrino–electron scattering for ^{7}Be neutrinos.

(v) ϕ^{Ga}, the measurement of the solar neutrino flux using inverse β decay in gallium [29]. This observable is sensitive to neutrinos produced in all distinct neutrino-producing fusion reactions, but only to the electron neutrino component of the solar neutrino flux.

(vi) ϕ^{Cl}, the measurement of the solar neutrino flux using inverse β decay in chlorine [30]. This observable is sensitive to neutrinos produced in all distinct neutrino-producing fusion reactions, except those involving the $p + p$ reaction, but only to the electron neutrino component of the solar neutrino flux.

All flux measurements are defined assuming that the incoming neutrinos are all electron neutrinos. For example,

$$\phi^{ES}(\text{Borexino}) = \frac{\phi_{^7\text{Be}}(\sigma_{\nu_e e} P_{ee} + \sigma_{\nu_a e} P_{ea})}{\sigma_{\nu_e e}}$$

$$= \phi_{^7\text{Be}}\left(P_{ee} + \frac{\sigma_{\nu_a e}}{\sigma_{\nu_e e}} P_{ea}\right), \qquad (3.18)$$

where $\phi_{^7\text{Be}}$ is the standard solar model expectation for the ^{7}Be solar neutrino flux and $\sigma_{\nu_\zeta e}$ is the cross section for elastic ζ-type neutrino–electron scattering, $\zeta = e, a$.

Before presenting the results of a χ^2 fit to the data spelled out above, it is illustrative to describe the dominant aspects of the data that constrain the presence of the extra mass-squared differences. For ^{8}B neutrinos, the combined

SNO and Super-Kamiokande data not only reveal that $P_{ee} \sim 0.3$ for neutrino energies above a few MeV, but also reveal that $P_{ea} \sim 0.7$. A more detailed analysis, presented in the Appendix, reveals that for ^{8}B neutrinos, $P_{es} < 0.37$ at the 3σ confidence level. As advertised, this rules out at least $\epsilon \gtrsim 10^{-3}$ in the $2 + 1$ case [see Eq. (3.10)]. Upon further scrutiny, it is easy to see that, for $\epsilon \gtrsim 10^{-6}$, $P_{es} \sim 0.5$ in the $2 + 1$ case, which is ruled out by the current data.

For solar neutrino energies below 1 MeV or so, information regarding neutrino oscillations is dominated by Borexino, the Homestake experiment, and the gallium experiments. The Borexino experiment measures, with good precision, mostly for ^{7}Be solar neutrinos ($E_\nu = 0.862$ MeV), $P_{ee} = 0.56 \pm 0.10$ in the limit $P_{es} \rightarrow 0$ [31]. For larger values of P_{es}, P_{ee} is driven towards higher values in order to compensate for the depletion of the ν_a component of the ^{7}Be solar neutrino flux at the earth. This effect is depicted in more detail in the Appendix. For lower energy neutrinos, the gallium experiments, taking into account the data, mostly, from Borexino, SNO, and Super-Kamiokande, constrain $P_{ee} \sim 0.55$ for pp neutrinos, and are insensitive to whether those convert into active or sterile neutrinos.[8]

Figure 5 depicts $\Delta\chi^2 = \chi^2 - \chi^2$ ($\epsilon = 0$) as a function of ϵ, in the case of two active and one sterile neutrino, for $m^2 = 7.6 \times 10^{-5}$ eV^2 and $\sin^2\theta = 0.31$. χ^2 is the result of a χ^2 fit to the data described above, and we will use it in order to establish an upper bound on ϵ. More specifically, we will state that values of ϵ associated to $\Delta\chi^2 > 4, 9$ are ruled out at the two, three sigma level. While we quote a bound for a fixed value of m^2, $\sin^2\theta$, we have verified that a very similar bound is obtained for different values of these oscillation parameters (in which case we also include the measurement of m^2 from the KamLAND experiment in the χ^2 function). We note, for example, that there is no good fit for values of θ outside the currently best fit region for $\sin^2\theta_{12}$ [21], even if one considers significant values of ϵ. From the figure, we estimate that the largest value of ϵ allowed at the three sigma level is $\epsilon < 2.0 \times 10^{-7}$, while at the two sigma level $\epsilon < 1.2 \times 10^{-7}$. Furthermore, the region $2.4 \times 10^{-8} < \epsilon < 7.1 \times 10^{-8}$ is ruled out at the two sigma level. In this region P_{es} is large for solar neutrino energies around 1 MeV, while P_{ee} is less than one-half, in contradiction with the Borexino data. For slightly larger values of ϵ, the peak in P_{es} moves to solar neutrino energies larger than 1 MeV but smaller than the threshold for the SNO and Super-Kamiokande experiments, where there is virtually no experimental informa-

---

[7]Borexino is also sensitive to neutrinos produced in the CNO cycle. These account for around 10% of the neutrinos with energies around those of the ^{7}Be neutrinos and have been neglected. The current Borexino data are consistent with a vanishing CNO neutrino flux [31].

[8]The bound on P_{ee} depends indirectly on P_{es} for higher energy neutrinos as these modify the measurement of P_{ee} for the high-energy neutrinos and hence the extraction of P_{ee} for pp neutrinos from the gallium data. Details are provided in the Appendix.
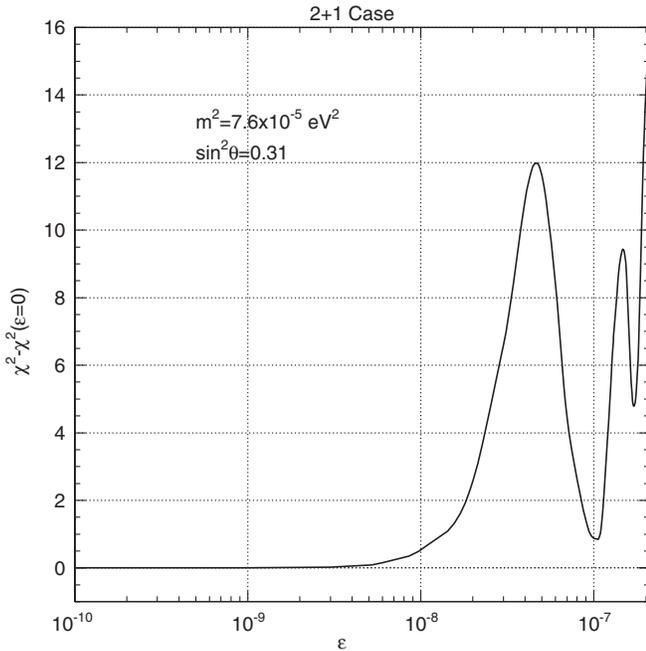
FIG. 5. $\chi^2 - \chi^2$ ($\epsilon = 0$) as a function of ϵ for $m^2 = 7.6 \times 10^{-5}$ eV^2, $\sin^2\theta = 0.31$, in the 2 + 1 case.

tion. In this case, the fit to the data is just as good as the one obtained for $\epsilon = 0$.

It is also worthwhile pointing out that, for $\epsilon \sim 1 \times 10^{-7}$, P_{ee} for ^{8}B neutrinos is expected to be mostly constant as a function of energy, contrary to the standard LMA case, where a slight decrease of P_{ee} as a function of energy is expected. This behavior is observed for the appropriate parameter choices in other ''new physics'' scenarios including nonstandard neutrino interactions [33], mass-varying neutrinos [34], and the introduction of light sterile neutrinos that mix very weakly with active ones [35]. Such a behavior was advertised as solution to the fact that the ^{7}Be electron neutrino flux, extracted using the chlorine data, was lower than the one predicted by the canonical LMA solution to the solar neutrino puzzle. This tension in the data has been significantly relaxed with the introduction of those from Borexino.

The bounds above translate into $2m^2\epsilon < (1.8, 3.0) \times 10^{-11}$ eV^2 as the two, three sigma upper bound on the induced small mass-squared difference and $\epsilon_m < (1.0, 1.7) \times 10^{-9}$ eV at the two, three sigma level. Note that our bounds agree qualitatively with those obtained, under slightly different circumstances and after some re-interpretation of the relevant observables, in [20]. The analysis in [20] did not include results from Borexino, not available before 2008.

In the 2 + 2 case, we wish to place bounds on both ϵ_1 and ϵ_2, and discuss which between $\epsilon_{m1} = m_1\epsilon_1$ and $\epsilon_{m2} = m_2\epsilon_2$ is more severely constrained. Unlike the 2 + 1 case, the data (mostly from KamLAND) do not specify m_1^2 or m_2^2, but constrain $m_2^2 - m_1^2 = 7.6 \times 10^{-5}$ eV^2. As dis-

cussed in the previous subsection, the solar data constrain $m_1^2\epsilon_1$ and $m_2^2\epsilon_2$. Keeping all this in mind, we will first discuss the bounds of ϵ_1 and ϵ_2 for fixed $m_1^2 = 1.0 \times 10^{-6}$ eV^2 and $m_2^2 = 7.7 \times 10^{-5}$ eV^2 and then discuss the bounds on ϵ_m for various values of m_1^2, m_2^2 by varying these two masses while maintaining $m_2^2 - m_1^2$ constant and in agreement with the KamLAND data. As in the 2 + 1 case, we will discuss bounds for fixed $m_2^2 - m_1^2 = 7.6 \times 10^{-5}$ eV^2 and $\sin^2\theta = 0.31$. We have checked that a very similar bound is obtained when one allows these two parameters to vary in the fit.

In more detail, we describe the bounds on ϵ_1 in the limit of very small ϵ_2 and vice versa. The reason for doing this is that $\epsilon_1 \times \epsilon_2$ correlated effects are not very large. In the limit where ϵ_1 effects are negligible, ϵ_2 bounds are similar to those on ϵ in the 2 + 1 case. In more detail, $2m_2^2\epsilon_2 < 3.0 \times 10^{-11}$ eV^2 at the three sigma level. In the limit where ϵ_2 effects are negligible, we obtain, following a procedure identical to the one discussed in the 2 + 1 case above, $\epsilon_1 < 5.3 \times 10^{-7}$ at the two sigma level and $\epsilon_1 < 8.8 \times 10^{-7}$ at the three sigma level for $m_1^2 = 1.0 \times 10^{-6}$ eV^2. This translates into a new mass-squared difference $2m_1^2\epsilon_1 < (1.1, 1.8) \times 10^{-12}$ eV^2 at the two, three sigma level.

We are interested in upper bounds for the elements of ϵ_m. From the bounds on the mass-squared differences above, we obtain, at the three sigma level,

$$\epsilon_{m1} < 8.8 \times 10^{-10} \text{ eV}\left(\frac{10^{-3} \text{ eV}}{m_1}\right), \qquad (3.19)$$

$$\epsilon_{m2} < 1.7 \times 10^{-9} \text{ eV}\left(\frac{8.8 \times 10^{-3} \text{ eV}}{m_2}\right). \qquad (3.20)$$

These bounds are obtained for $\sin^2\theta = 0.31$ and $m_2^2 - m_1^2 = 7.6 \times 10^{-5}$ eV^2 and are hence correlated. In the case of an inverted mass hierarchy, for example, if $m_1 = 50.000 \times 10^{-3}$ eV while $m_2 = 50.076 \times 10^{-3}$ eV, the three sigma bounds above translate into $\epsilon_{m1} < 1.8 \times 10^{-11}$ eV and $\epsilon_{m2} < 3.0 \times 10^{-10}$ eV. On the flip side, while $m_2^2 > 7.6 \times 10^{-5}$ eV^2 is bounded from below, m_1 can be arbitrarily small, which indicates that the upper bound on ϵ_{m1}, while naively stronger than that on ϵ_{m2}, could be significantly worse.[9]

Before moving on to current nonsolar and future constraints on ϵ_m, we would like to emphasize a few relevant points. We have not considered earth matter effects while

---

[9]Strictly speaking, some of the approximations made in Sec. II fail when m_1 is of order ϵ_{m1} and hence the bound Eq. (3.19) is not applicable when $m_1 \lesssim 10^{-6}$ eV. In this case however, the generic upper bound on ϵ_m, as discussed in the introduction to Sec. III is dominated by Eq. (3.20). For even smaller values of $m_1 \lesssim 10^{-9}$ eV we anticipate that there are no relevant effects due to the fact that our approximations fail. On the contrary, in this case we expect oscillations due to sterile effects to be entirely dominated by the 2 + 1 case discussed here.

computing our oscillation probabilities, neither have we worried about large seasonal variations of the solar neutrino flux induced by the very large oscillation length induced by the new, very small mass-squared differences. The fact that we can ignore day–night effects is justified *a posteriori*. Earth matter effects are most significant when the matter potential of the earth is of order $\Delta m^2 / 2E$. For ^{7}Be neutrinos ($E = 0.862$ MeV) large (more than 1%) day–night effects are expected for $\Delta m^2 \gtrsim 10^{-8}$ eV^2 (see, for example, [36]), so we estimate that, for solar neutrino energies above 100 keV (below the threshold of the gallium experiments), large day–night effects are expected for $\Delta m^2 \gtrsim 10^{-9}$ eV^2. This is 2 orders of magnitude larger than the worse upper obtained for $|m_2^2 - m_{2'}^2|$. These estimates are in agreement with more detailed computations performed in [20]. Seasonal variations, on the other hand, are expected for $E \lesssim 1$ MeV if the bounds on ϵ_m are saturated. These could be observed in, for example, the Borexino experiment. For an estimate of how large an effect one may hope to observe, we point readers to [20,37].

IV. OTHER CONSEQUENCES AND FUTURE SENSITIVITY

Whether the neutrinos are Dirac or pseudo-Dirac fermions is a notoriously difficult issue to resolve, especially in the limit when the right-handed neutrino mass matrix ϵ_m is tiny. Other than observing the long-wavelength oscillation driven by the new mass-squared differences between the quasidegenerate mass-squared states, it seems virtually impossible to construct observables that will reveal the pseudo-Dirac nature of the neutrinos.

It is well-known that for pseudo-Dirac neutrinos which arise from a seesaw Lagrangian [Eq. (1.1)] the neutrino exchange contribution to neutrinoless double-beta decay vanishes almost perfectly [17]. One way of understanding this is to note that the contributions of the different quasidegenerate states to neutrinoless double-beta decay are equal and opposite, and cancel pairwise. Another way of appreciating this fact is to see that, when all neutrinos are lighter than tens of MeV, the rate for neutrinoless double-beta decay is proportional to the *ee* element of the full neutrino mass matrix, which, as one can quickly read off Eq. (2.1), is exactly zero. This "property" is present even when the neutrinos are not pseudo-Dirac states, and depends only on all right-handed neutrino masses being small enough [8,9]. For the same reason, "all" (for a long list of observables see, for example, [38]) potentially observable lepton-number violating phenomena are also guaranteed to vanish almost perfectly if the only sources of lepton-number violation are the Majorana neutrino masses. As far as kinematical probes of the neutrino masses are concerned—the most stringent laboratory bounds come from tritium beta-decay experiments [19]—the neutrinos behave as if they were Dirac fermions, their "pseudo" nature

completely obscured by the very stringent constraints from oscillation experiments.

One also needs to consider cosmological bounds on the number of neutrino species since, in the scenarios considered here, there are five or six light neutrinos compared with three in the case of, say, a high-scale version of the seesaw mechanism ($M \gg 100$ GeV, where M are the right-handed neutrino Majorana mass parameters). Again, the situation here is, in practice, indistinguishable from the case of Dirac neutrinos. It is well-known that in the case of light neutrinos, cosmological bounds on the number of light degrees of freedom cannot distinguish three light Majorana from three light Dirac neutrinos. The reason is that neutrino masses are very small and right-handed neutrinos are gauge singlets, meaning that, in the early universe, the right-handed neutrino degrees of freedom, which exist in the case of Dirac neutrinos, are not populated. In the pseudo-Dirac scenarios we are considering here, the situation is very similar. For small enough right-handed neutrino masses, the sterile neutrinos are too weakly coupled and their states are not significantly populated in the early universe [20,39,40]. Given the bounds obtained in the previous case, this is exactly the case, and we do not expect any observable consequence of the new light degrees of freedom as far as cosmological observables are concerned.

In the near future, current solar neutrino experiments are expected to improve our understanding of very small right-handed neutrino masses. Borexino will accumulate more data (and their systematic uncertainties are expected to go down) and improve on their results published in [31]. As mentioned above, Borexino is expected to measure the solar neutrino flux as a function of time, and may be sensitive to anomalous seasonal variations. The absence of such effects should help erase the local minimum around $\epsilon = 1 \times 10^{-7}$ in the $2 + 1$ $\Delta \chi^2$ function, depicted in Fig. 5, and improve on the bound on ϵ (ϵ_2) in the $2 + 1$ ($2 + 2$) case. It is also expected that SNO and Super-Kamiokande will be able to access the low-energy end ($E < 5$ MeV) of the ^{8}B solar neutrino spectrum and shed more light on the expected (from the canonical LMA solution) rise in P_{ee} as the neutrino energy decreases.

Future neutrino experiments are aimed at measuring with more precision (and in real time) the pp solar neutrino flux and that of the pep and CNO neutrinos [41]. These would not only provide a more precise measurement of P_{ee} for very low-energy solar neutrinos (the pp neutrinos, $E \lesssim 0.5$ MeV) but would also fill the energy "gap" between ^{7}Be neutrinos and ^{8}B neutrinos (the pep and CNO neutrinos, $E \sim 1$–2 MeV). Indeed, Borexino is currently working on controlling the cosmogenic ^{11}C background in order to access the pep and CNO neutrino fluxes. It is expected that such results, if consistent with the canonical LMA solution to the solar neutrino puzzle, will improve, perhaps by an order of magnitude, the bounds on ϵ in the

$2 + 1$ case or $\epsilon_{1,2}$ in the $2 + 2$ case discussed in the previous section.

Access to new neutrino oscillation lengths much longer than the earth–sun distance will only be provided by astrophysical neutrinos, which travel galactic and extragalactic distances. In particular, it has been pointed out [42] that studies of the flavor composition of ultrahigh energy neutrinos, to which neutrino telescopes are sensitive, are sensitive to the new mass-squared differences that characterize pseudo-Dirac neutrinos if these are as small as 10^{-16} eV^2 or perhaps 10^{-18} eV^2. Taking these estimates at face value, one would be sensitive to right-handed neutrino masses

$$\epsilon_m > 1.1 \times 10^{-17} \left(\frac{\delta m^2}{10^{-18} \text{ eV}^2} \right) \text{ eV}, \qquad (4.1)$$

where δm^2 is the mass-squared difference which can be potentially accessed by neutrino telescopes [42]. The sensitivity above is estimated in the limit where $m_3^2 = 2 \times 10^{-3}$ eV^2 (in which case the neutrino mass hierarchy is normal) and is expected to be more inclusive if all neutrino masses are larger, as was observed in the $2 + 2$ analysis in the previous section.

V. SUMMARY, CONCLUDING THOUGHTS

The addition of gauge-singlet Weyl fermions to the standard model Lagrangian is a very simple and effective way of rendering the neutrinos massive, as required by experimental observations. The most general renormalizable Lagrangian consistent with this enlarged particle content, Eq. (1.1), while deceptively simple, provides a colorful spectrum of different phenomenological consequences, depending on the values of the new parameters in the νSM.

For any value of the parameters M_{ij} (gauge-singlet Majorana mass parameters), it is possible to obtain mostly active neutrino masses in the range highlighted by experiments by properly adjusting the value of the Yukawa couplings $\lambda_{\alpha i}$. It is, hence, sufficient to discuss the different phenomenological opportunities for testing the νSM as a function of M_{ij}. Further simplifying our discussion, we will consider that all M_{ij} are of the same order of magnitude, and will refer to all of them as M.

The largest allowed value of M is of order 10^{15} GeV [43]. This comes from the requirement that Eq. (1.1) is appropriate to describe physics at energy scales of order M (unitarity and perturbativity). At these high energies (and all the way down to M values of order the weak scale) the only directly observable consequences of Eq. (1.1) are the small Majorana masses of the mostly active neutrinos. More indirectly, lepton-number violating processes involving gauge-singlet fermions in the early universe may be responsible for the matter-antimatter asymmetry of the universe, through the leptogenesis mechanism [44].

For weak-scale M values ($1 \text{ MeV} \lesssim M \lesssim 100 \text{ GeV}$) the theory contains new neutral heavy leptons, which are, predominantly, gauge-singlet fermions which should be produced in a variety of weak processes including charged-lepton and meson decays (see, for example, [11,12,14]). These neutral heavy leptons should also be produced in collider experiments, and in principle, their decays should point to lepton-number violation at colliders [45]. Indirectly, the presence of neutral heavy leptons is expected to mediate charged-lepton flavor violating phenomena and the apparent violation of universality of the weak coupling constant and of unitarity of the neutrino mixing matrix. Whether any of these phenomena are observable in practice depends on the amount of mixing between the active neutrinos $\nu_{a=e,\mu,\tau}$ and the gauge-singlet fermions, $\nu_{s=s_1,s_2,\ldots}$. Figure 6 depicts a naive estimate, as a function of M, of this mixing angle $\sin^2\theta_{as}$ given by Eq. (1.1). In the limit $M \gg m_\nu$,

$$\sin^2\theta_{as} \equiv \frac{m_\nu}{M}, \qquad (5.1)$$

where m_ν are the mostly active neutrino masses (m_1, m_2, m_3, constrained by oscillation experiments). The figure depicts $\sin^2\theta_{as}$ for three different values of the mostly active neutrino masses, according to guidance provided by the current neutrino data. Experiments are sensitive to neutral heavy leptons if $\sin^2\theta_{as} \gtrsim 10^{-4}$ (best case scenario), which leads one to naively conclude that Eq. (1.1), if responsible for the observed neutrino masses, cannot be tested experimentally for M values in this range ($1 \text{ MeV} \lesssim M \lesssim 100 \text{ GeV}$). It is, however, important to emphasize that Eq. (5.1) can be violated and much larger $\sin^2\theta_{as}$ values are consistent with the oscillation data [14,15]. Whether this possibility is realized in nature can only be established experimentally.

Sub-MeV neutral heavy leptons ($1 \text{ eV} \lesssim M \lesssim 1 \text{ MeV}$) can make their presence known in astrophysics, cosmol-
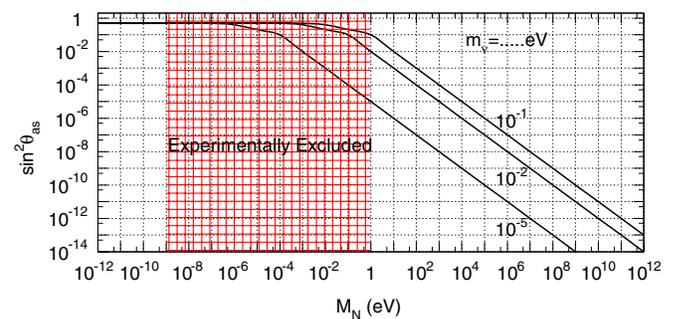

FIG. 6 (color online). Estimate of the magnitude of the mixing between active and sterile neutrinos $\sin^2\theta_{as}$ as a function of the right-handed neutrino mass M_N, for different values of the mostly active neutrino masses, $m_\nu = 10^{-1}$, 10^{-2}, and 10^{-5} eV. The hatched region qualitatively indicates the values of M_N that are currently excluded by the world's particle physics data.

ogy, and neutrino oscillation experiments. If M values are in this range, it also turns out that, while neutrinos are Majorana fermions, the expected rates for all potentially observable lepton-number violating phenomena are strongly suppressed, as the contributions from the mostly active states cancel those from the mostly sterile ones [8,9]. In this mass range, mostly sterile neutrinos become an interesting dark matter candidate [13], and at the same time, part of this mass region is only allowed if one can bypass cosmological constraints on the number of neutrino species [9].

In this paper, we were interested in new light neutrinos, or small values of M (zero $\lesssim M \lesssim 1$ eV). In this case, Eq. (5.1) does not apply at all, and active–sterile neutrino mixing is naively expected to be large. M values of order the active neutrino masses m_1, m_2, m_3 are most likely excluded by failed searches for sterile neutrinos in oscillation experiments. A detailed discussion of this parameter region is very dependent on the structure of the Yukawa matrix λ and is not the subject of this paper. Instead, we concentrated in the limit $M \ll m_1, m_2, m_3$.

If the gauge-singlet Majorana neutrino masses are much smaller than the Dirac neutrino masses $m_{\alpha i} = \lambda_{\alpha i} v$, where v is the vacuum expectation value of the neutral component of the Higgs doublet, neutrinos are classified as pseudo-Dirac neutrinos. When $M_{ij} = 0$ for all i, j, neutrinos are Dirac fermions and all experimental data can be accommodated perfectly. For $M_{ij} \neq 0$ but small enough, this conclusion remains true. Our goal was to estimate above what small but nonzero value of M_{ij} is Eq. (1.1) ruled out by experimental data. We find that the most stringent constraints come from the current solar neutrino data. The most conservative upper bound on the best constrained element of the gauge-singlet Majorana mass matrix, in the basis defined in Sec. II, is $M < 1.7 \times 10^{-9}$ eV at the three sigma confidence level. This bound is significantly stronger if the neutrino mass hierarchy is inverted or if the lightest neutrino mass (m_1 in the case of a normal mass hierarchy) is larger than 10^{-3} eV.

The hatched region in Fig. 6 indicates the values of M for which Eq. (1.1) is excluded as an explanation for the nonzero neutrino masses. It is remarkable that while providing a good quantitative fit to all particle physics data, the parameters of Eq. (1.1) are only miserably constrained. All available neutrino data allow one to "measure" $M \in [0, 10^{-9}]$ eV $\cup$ $M \in [10^{-9}, 10^{15}]$ GeV, while the largest $\lambda_{\alpha i} \in [2 \times 10^{-13}, 10]$. It is clear that we have only begun to properly probe the origin of neutrino masses.

If neutrino masses are indeed a consequence of Eq. (1.1) with $M \lesssim 10^{-9}$ eV, this and the next generation of solar neutrino experiments, especially those aiming at the pp, ^{7}Be, and pep solar neutrinos, will provide positive evidence for new very light neutrinos and new very small mass-squared different, as long as the right-handed neutrino Majorana mass parameters are not much smaller (say,

an order of magnitude) than the upper bounds discussed here. The evidence for new neutrino degrees of freedom would manifest itself via a significant difference between future experimental observations and expectations from the standard LMA solution to the solar neutrino puzzle. By carefully mapping the electron neutrino survival probability as a function of energy one should be able to determine some of the elements of the right-handed neutrino Majorana mass matrix. If the model discussed here is indeed realized in nature but M values are too small and outside the reach of solar neutrino experiments (defined by the earth–sun distance and the solar neutrino energy spectrum), the pseudo-Dirac nature of the neutrinos may still manifest itself in studies of ultrahigh energy neutrinos of extragalactic origin, as discussed in Sec. IV.

Finally, if neutrino masses are a consequence of the existence of new gauge-singlet degrees of freedom N with very small Majorana masses M [Eq. (1.1) with $M \ll \lambda v$], one will still have to contend with two "numerological" puzzles: why are the neutrino Yukawa couplings so small, and why are the right-handed neutrino Majorana masses less than, say, 10^{-9} eV? Several mechanisms have been proposed in the literature in order to explain very small neutrino Yukawa couplings, including models with extra space dimensions (of the flat and the warped varieties) [46] and models with new, spontaneously broken symmetries (see, for example, [47]). Explaining why the right-handed neutrino Majorana masses are small is, in principle, a different kind of question. Since M is the coefficient of a relevant operator in the Lagrangian, it is not clear what its natural value should be. It has already been argued that M is a symmetry breaking parameter [Eq. (1.1) is invariant under $U(1)_{B-L}$ when all $M_{ij} = 0$] and hence any value it happens to have is stable against quantum corrections and hence technically natural as defined by 't Hooft. Regardless, there are several mechanisms identified in the literature that "explain" why right-handed neutrino masses might be much smaller than the Planck, grand unified theory, or even the weak scale (see, for example, [48]).

For concreteness, we provide here a naive toy example inspired by scenarios discussed in [47,48]. Imagine that the N fields are charged under a new symmetry such that both the neutrino Yukawa couplings and the right-handed neutrino Majorana masses are forbidden, but introduce a new scalar field S with quantum numbers such that NS is invariant under the new symmetry. We also need to postulate that $U(1)_{B-L}$ is spontaneously broken by the vacuum expectation value of some field X (with lepton number 2). In this case, the following dimension-five nonrenormalizable operators are allowed, after $U(1)_{B-L}$ breaking:

$$\mathcal{L}_{\nu SM} = \mathcal{L}_{old} - \varepsilon \frac{f_{\alpha\beta}}{2\Lambda}(L^\alpha H)(L^\beta H) - \frac{y_{\alpha i}}{\Lambda}(L^\alpha H)(N^i S)$$
$$- \varepsilon \frac{\omega_{ij}}{2\Lambda}(N^i S)(N^j S) + \text{H.c.}, \tag{5.2}$$

where f, y, ω are dimensionless couplings (say, of order one), Λ is the scale of new physics, and $\epsilon = \langle X \rangle / \Lambda'$ (Λ need not be the same as Λ'). In this case, after S and H get vacuum expectation values s and v, respectively, we are left with Eq. (2.1) where

$$m = \frac{vs}{\Lambda} y, \qquad \epsilon_m = \epsilon \frac{s^2}{\Lambda} \omega, \qquad 0_3 \rightarrow \epsilon \frac{v^2}{\Lambda} f. \quad (5.3)$$

The scenario discussed in this paper is realized when $s \gg v$ (so that 0_3 can be ignored) and $v/s \gg \epsilon$ so that $m \gg \epsilon_m$ (pseudo-Dirac condition).

Before concluding, we would like to highlight that in Sec. II we discussed a very useful basis in which to describe pseudo-Dirac neutrinos. In the basis of choice, the relation between the mass-squared splittings of the different quasidegenerate states is directly related to the "diagonal" elements of M_{ij}, while the "off-diagonal" ones are only responsible, at leading order, for affecting the neutrino mixing matrix. Bounds on these off-diagonal elements were not discussed in any detail, but we argued that these are much weaker than the bounds on the diagonal elements. It is worthwhile to investigate how such effects might be probed experimentally.

ACKNOWLEDGMENTS

APPENDIX: MODEL INDEPENDENT FIT TO SOLAR NEUTRINO DATA, INCLUDING STERILE NEUTRINOS

In this Appendix, we discuss a model independent, simplified fit to the solar neutrino data, along the lines of analyses performed in the past by Barger, Marfatia, and Whisnant [49,50]. In a nutshell, we split the oscillation probabilities of solar neutrinos into three disjoined regions, qualitatively constrained by different experiments:

(i) P^H: this is the oscillation probability of high-energy solar neutrinos ($E > 4$ MeV), averaged over the entire energy region. In practice, P^H is dominated by the ^{8}B neutrinos, and is, by far, best constrained by the real time experiments Super-Kamiokande and SNO.

(ii) P^M: this is the oscillation probability of medium energy solar neutrinos ($0.5 < E < 4$ MeV). In practice, constraints on this region are dominated by the monochromatic ^{7}Be neutrinos ($E = 0.863$ MeV). P^M is best constrained by the Borexino experiment.

(iii) P^L: this is the oscillation probability of the low-energy solar neutrinos ($E < 0.5$ MeV). These con-

sist almost exclusively of pp neutrinos and are only constrained by the gallium experiments.

Our analysis is very similar to that of [49,50], to which we refer for details, with two exceptions. One is that the Borexino data were not available when [50] was published and we discuss their impact here. The other is that we wish to consider that the electron neutrinos can oscillate into sterile neutrinos, and discuss how constrained is this possibility.

Figure 7 depicts the allowed region of the $P_{es}^H \times P_{ee}^H$ parameter space at different confidence levels after combining data from Super-Kamiokande [28] and SNO [27]. From the SNO experiment we learn $\phi^{CC} = (1.67 \pm 0.09) \times 10^6$ cm^{-2} s^{-1}, $\phi^{NC} = (5.54 \pm 0.48) \times 10^6$ cm^{-2} s^{-1}, while from Super-Kamiokande we learn $\phi^{ES} = (2.35 \pm 0.08) \times 10^6$ cm^{-2} s^{-1}. For the standard solar model expectation we assume $\phi = (5.69 \pm 0.91) \times 10^6$ cm^{-2} s^{-1}. We picked the theoretical prediction that leads to the most conservative bound on P_{es}^H and assumed $P_{ee}^H + P_{es}^H + P_{ea}^H = 1$. After marginalizing over P_{ee}^H values, we obtain $P_{es}^H \in [0, 0.37]$ at the three sigma level.

Figure 8 depicts the allowed region of the $P_{es}^M \times P_{ee}^M$ parameter space at different confidence levels after combining data from Borexino [31] and the Homestake experiments [30]. While computing the expected flux at Homestake, we use the value of P_{ee}^H obtained in the analysis depicted in Fig. 7 in order to estimate the contribution of ^{8}B neutrinos to the neutrino flux measured at Homestake. For more details regarding how to treat the chlorine data, we refer readers to [49,50]. For the Borexino experiment, we learn that 49 ± 5 counts/day/100 tons are
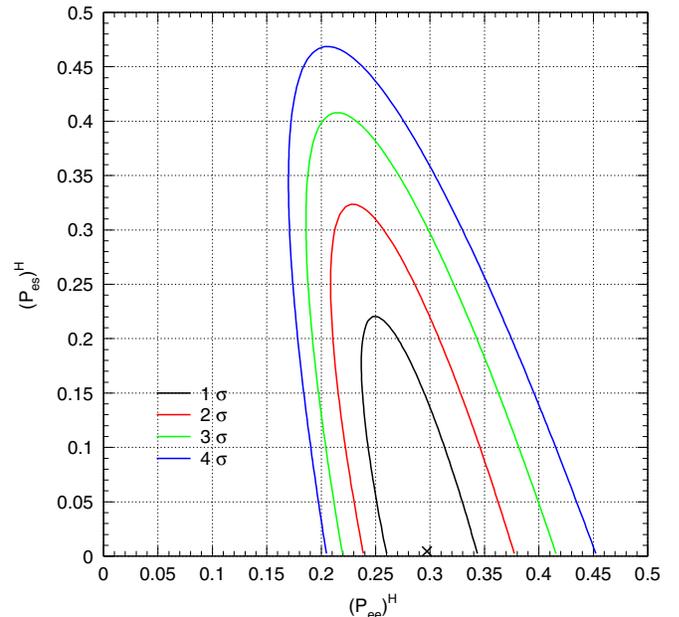

FIG. 7 (color online). Allowed region of the $P_{es}^H \times P_{ee}^H$ parameter space after combining data from Super-Kamiokande and SNO experiments at the 1, 2, 3, and 4 σ levels. Confidence levels are defined as regions of constant $\Delta\chi^2 = 2.3, 6.18, 11.83, 17.95$.
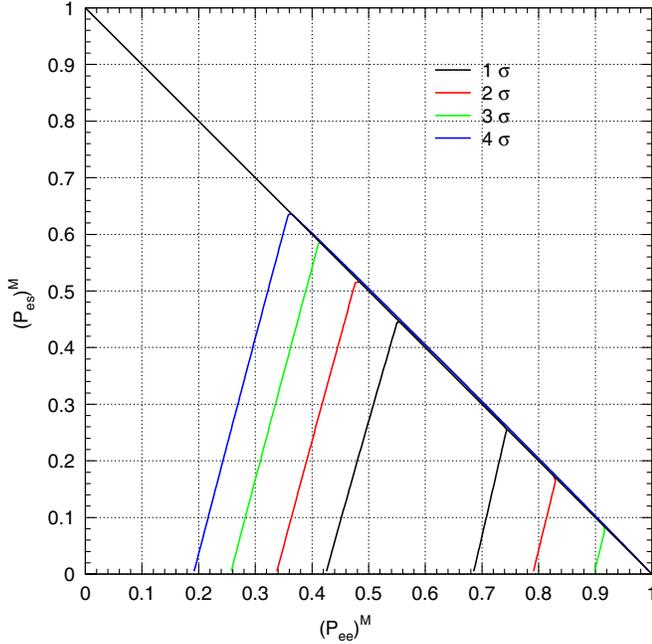
FIG. 8 (color online). Allowed region of the $P_{es}^M \times P_{ee}^M$ parameter space after combining data from Borexino and the Homestake experiments at the 1, 2, 3, and 4 σ levels. Confidence levels are defined as regions of constant $\Delta\chi^2 = 2.3, 6.18, 11.83, 17.95$.
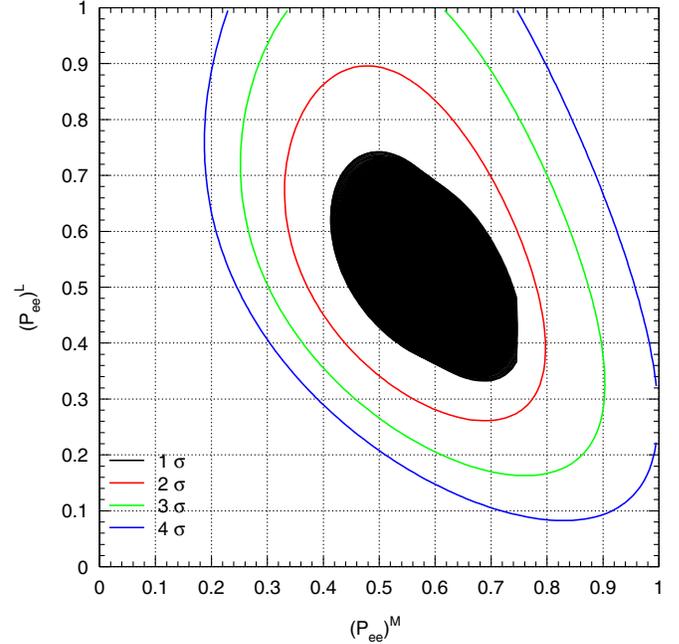

FIG. 9 (color online). Allowed region of the $P_{ee}^L \times P_{ee}^M$ parameter space after combining data from Borexino and the Homestake experiments at the 2, 3, and 4 σ levels (lines), assuming $P_{es}^M = 0$, and at the 1σ confidence level (boundary of the solid black region) marginalizing over all allowed P_{es}^M values (see Fig. 8). Confidence levels are defined as regions of constant $\Delta\chi^2 = 2.3, 6.18, 11.83, 17.95$.

observed, while 75 ± 4 counts/day/100 tons were expected according to the standard solar model. The constraint $P_{ee}^M + P_{es}^M + P_{ea}^M = 1$ "cuts off" the part of the parameter space where $P_{ee}^M + P_{es}^M > 1$. Note that our confidence level curves are defined as constant $\Delta\chi^2 \equiv \chi^2(P_{ee}^M, P_{es}^M) - \chi^2_{\min}$ contours. One should hence be careful when translating what we refer to as an N sigma ($N = 1, 2, 3, \dots$) bound into a probability that a certain value is allowed. Marginalizing over P_{ee}^M, we get $P_{es}^M \in [0, 0.57]$ at the three sigma confidence level.

It is interesting to note that, similar to the neutral current measurement at SNO and the elastic scattering result from Super-Kamiokande, the Borexino result is sensitive to both electron neutrinos and other active ($\nu_{\mu,\tau}$) neutrino species, but Borexino data alone cannot rule out $P_{ea}^M = 0$. In principle, the combination of Borexino and Homestake data is sensitive to whether $P_{ea}^M \neq 0$. Alas, this is not the case in practice, as one can readily see in Fig. 8.

As noted above, all information on low-energy neutrinos comes from the gallium experiments, and these are only sensitive to P_{ee} (i.e., the gallium experiments are only sensitive to electron neutrinos from the sun). On the other hand, since the gallium experiments are sensitive to neutrinos of all energies above the experimental threshold, the

gallium result for P_{ee}^L depends on P_{ee}^M and P_{ee}^H. P_{ee}^H is well constrained by the ^{8}B experiments, so we concentrate on the interplay between P_{ee}^L, P_{ee}^M and P_{es}^M (note that there is no experimental information on P_{es}^L or P_{ea}^L). Figure 9 depicts the allowed region of the $P_{ee}^L \times P_{ee}^M$ parameter space after combining data from the Borexino and gallium experiments (the contribution from Homestake data is also included. Its effect is very small). In order to illustrate the effect of sterile neutrinos, the figure depicts the one sigma allowed region obtained once we marginalize over all allowed values of P_{es}^M (boundary of the black region in Fig. 9) and the two, three, and four sigma allowed regions which are obtained if P_{es}^M is set to zero in the analysis.

Our result is consistent with that shown by the Borexino Collaboration in the Neutrino 2008 conference [51]. It also depicts the correlation between P_{ee}^L and P_{ee}^M, courtesy of the gallium experiments. Finally the presence of sterile neutrinos in the fit renders the allowed region in the $P_{ee}^L \times P_{ee}^M$ plane larger, but does not qualitatively invalidate the results obtained assuming that there are no sterile neutrinos.

[1] M. C. Gonzalez-Garcia and M. Maltoni, Phys. Rep. **460**, 1 (2008).

[2] J. W. F. Valle, J. Phys. Conf. Ser. **53**, 473 (2006).

[3] A. Strumia and F. Vissani, arXiv:hep-ph/0606054.

[4] R. N. Mohapatra and A. Y. Smirnov, Annu. Rev. Nucl. Part. Sci. **56**, 569 (2006).

[5] R. N. Mohapatra *et al.*, Rep. Prog. Phys. **70**, 1757 (2007).

[6] A. de Gouvêa, Mod. Phys. Lett. A **19**, 2799 (2004).

[7] A. de Gouvêa, arXiv:hep-ph/0411274.

[8] A. de Gouvêa, Phys. Rev. D **72**, 033005 (2005).

[9] A. de Gouvêa, J. Jenkins, and N. Vasudevan, Phys. Rev. D **75**, 013003 (2007).

[10] P. Minkowski, Phys. Lett. **67B**, 421 (1977); M. Gell-Mann, P. Ramond, and R. Slansky, in *Supergravity*, edited by D. Freedman and P. Van Niuwenhuizen (North Holland, Amsterdam, 1979), p. 315; T. Yanagida, in *Proceedings of the Workshop on Unified Theory and Baryon Number in the Universe*, edited by O. Sawada and A. Sugamoto (KEK, Tsukuba, Japan, 1979); S. L. Glashow, *1979 Cargèse Lectures in Physics—Quarks and Leptons*, edited by M. Lévy *et al.* (Plenum, New York, 1980), p. 707; R. N. Mohapatra and G. Senjanović, Phys. Rev. Lett. **44**, 912 (1980); J. Schechter and J. W. F. Valle, Phys. Rev. D **22**, 2227 (1980).

[11] D. Gorbunov and M. Shaposhnikov, J. High Energy Phys. 10 (2007) 015.

[12] See, for example, A. Yu. Smirnov and R. Zukanovich Funchal, Phys. Rev. D **74**, 013001 (2006); A. Atre, T. Han, S. Pascoli, and B. Zhang, J. High Energy Phys. 05 (2009) 030.

[13] T. Asaka, S. Blanchet, and M. Shaposhnikov, Phys. Lett. B **631**, 151 (2005).

[14] A. de Gouvêa, arXiv:0706.1732.

[15] J. Kersten and A. Yu. Smirnov, Phys. Rev. D **76**, 073005 (2007).

[16] L. Wolfenstein, Nucl. Phys. **B186**, 147 (1981); S. T. Petcov, Phys. Lett. **110B**, 245 (1982); S. M. Bilenky and B. Pontecorvo, Sov. J. Nucl. Phys. **38**, 248 (1983); Lett. Nuovo Cimento Soc. Ital. Fis. **37**, 467 (1983); Yad. Fiz. **38**, 415 (1983); **38**, 415 (1983).

[17] A. Halprin, S. T. Petcov, and S. P. Rosen, Phys. Lett. **125B**, 335 (1983); M. Doi, T. Kotani, and E. Takasugi, Prog. Theor. Phys. Suppl. **83**, 1 (1985).

[18] The literature on pseudo-Dirac neutrinos is vast. For an incomplete list of relevant, recent references, see, for example, G. J. Stephenson, J. T. Goldman, B. H. J. McKellar, and M. Garbutt, Int. J. Mod. Phys. A **20**, 6373 (2005); K. R. S. Balaji, A. Kalliomaki, and J. Maalampi, Phys. Lett. B **524**, 153 (2002); M. Kobayashi and C. S. Lim, Phys. Rev. D **64**, 013003 (2001); A. S. Joshipura and S. D. Rindani, Phys. Lett. B **494**, 114 (2000); U. Sarkar, Phys. Rev. D **59**, 037302 (1999); A. Geiser, Phys. Lett. B **444**, 358 (1998).

[19] C. Amsler *et al.* (Particle Data Group), Phys. Lett. B **667**, 1 (2008).

[20] M. Cirelli, G. Marandella, A. Strumia, and F. Vissani, Nucl. Phys. **B708**, 215 (2005).

[21] S. Abe *et al.* (KamLAND Collaboration), Phys. Rev. Lett. **100**, 221803 (2008).

[22] L. Wolfenstein, Phys. Rev. D **17**, 2369 (1978); S. P. Mikheev and A. Y. Smirnov, Yad. Fiz. **42**, 1441 (1985)

[Sov. J. Nucl. Phys. **42**, 913 (1985)]; Nuovo Cimento Soc. Ital. Fis. C **9**, 17 (1986).

[23] A. Friedland, Phys. Rev. D **64**, 013008 (2001).

[24] S. T. Petcov, Phys. Lett. B **200**, 373 (1988); S. Toshev, Phys. Lett. B **196**, 170 (1987).

[25] B. Aharmim *et al.* (SNO Collaboration), Phys. Rev. C **72**, 055502 (2005).

[26] B. Aharmim *et al.* (SNO Collaboration), Phys. Rev. C **75**, 045502 (2007).

[27] B. Aharmim *et al.* (SNO Collaboration), Phys. Rev. Lett. **101**, 111301 (2008).

[28] J. P. Cravens *et al.* (SuperKamiokaNDE Collaboration), Phys. Rev. D **78**, 032002 (2008).

[29] M. Altmann *et al.* (GNO Collaboration), Phys. Lett. B **616**, 174 (2005).

[30] B. T. Cleveland *et al.*, Astrophys. J. **496**, 505 (1998).

[31] C. Arpesella *et al.* (Borexino Collaboration), Phys. Rev. Lett. **101**, 091302 (2008).

[32] J. N. Bahcall, A. M. Serenelli, and S. Basu, Astrophys. J. **621**, L85 (2005); Astrophys. J. Suppl. Ser. **165**, 400 (2006).

[33] A. Friedland, C. Lunardini, and C. Pena-Garay, Phys. Lett. B **594**, 347 (2004).

[34] M. C. Gonzalez-Garcia, P. C. de Holanda, and R. Zukanovich Funchal, Phys. Rev. D **73**, 033008 (2006); M. Cirelli, M. C. Gonzalez-Garcia, and C. Pena-Garay, Nucl. Phys. **B719**, 219 (2005); V. Barger, P. Huber, and D. Marfatia, Phys. Rev. Lett. **95**, 211802 (2005).

[35] P. C. de Holanda and A. Y. Smirnov, Phys. Rev. D **69**, 113002 (2004).

[36] A. de Gouvêa, A. Friedland, and H. Murayama, J. High Energy Phys. 03 (2001) 009.

[37] A. de Gouvêa, A. Friedland, and H. Murayama, Phys. Rev. D **60**, 093011 (1999).

[38] A. de Gouvêa and J. Jenkins, Phys. Rev. D **77**, 013008 (2008).

[39] K. Enqvist, K. Kainulainen, and J. Maalampi, Phys. Lett. B **249**, 531 (1990).

[40] J. M. Cline, Phys. Rev. Lett. **68**, 3137 (1992).

[41] For a recent overview, see J. R. Klein, J. Phys. Conf. Ser. **136**, 022 004 (2008); associated slides at http://www2.phys.canterbury.ac.nz/~jaa53/presentations/J_Klein.pdf.

[42] J. F. Beacom, N. F. Bell, D. Hooper, J. G. Learned, S. Pakvasa, and T. J. Weiler, Phys. Rev. Lett. **92**, 011101 (2004); P. Keranen, J. Maalampi, M. Myyrylainen, and J. Riittinen, Phys. Lett. B **574**, 162 (2003).

[43] F. Maltoni, J. M. Niczyporuk, and S. Willenbrock, Phys. Rev. Lett. **86**, 212 (2001).

[44] M. Fukugita and T. Yanagida, Phys. Lett. B **174**, 45 (1986); for a recent overview, see S. Davidson, E. Nardi, and Y. Nir, Phys. Rep. **466**, 105 (2008).

[45] See, for example, O. Panella, M. Cannoni, C. Carimalo, and Y. N. Srivastava, Phys. Rev. D **65**, 035005 (2002); F. M. L. Almeida, Y. A. Coutinho, J. A. Martins Simões, and M. A. B. do Vale, Phys. Rev. D **62**, 075004 (2000); A. Datta, M. Guchait, and A. Pilaftsis, Phys. Rev. D **50**, 3195 (1994); T. Han and B. Zhang, Phys. Rev. Lett. **97**, 171804 (2006).

[46] See, for example, K. R. Dienes, E. Dudas, and T. Gherghetta, Nucl. Phys. **B557**, 25 (1999); Y. Grossman

and M. Neubert, Phys. Lett. B **474**, 361 (2000); G. Barenboim, G. C. Branco, A. de Gouvêa, and M. N. Rebelo, Phys. Rev. D **64**, 073005 (2001); A. de Gouvêa, G. F. Giudice, A. Strumia, and K. Tobe, Nucl. Phys. **B623**, 395 (2002); P. Q. Hung, Phys. Rev. D **67**, 095011 (2003).

[47] M. C. Chen, A. de Gouvêa, and B. A. Dobrescu, Phys. Rev. D **75**, 055009 (2007), and references therein.

[48] J. Sayre, S. Wiesenfeldt, and S. Willenbrock, Phys. Rev. D **72**, 015001 (2005).

[49] V. D. Barger, D. Marfatia, and K. Whisnant, Phys. Lett. B **509**, 19 (2001).

[50] V. Barger, D. Marfatia, and K. Whisnant, Phys. Lett. B **617**, 78 (2005).

[51] C. Galbiati (Borexino Collaboration), XXIII International Conference on Neutrino Physics and Astrophysics, Christchurch, New Zealand, 2008; Slides available at http://www2.phys.canterbury.ac.nz/~jaa53/presentations/ Galbiati.pdf.